Hindawi
International Journal of Aerospace Engineering
Volume 2022, Article ID 5899199, 22 pages
https://doi.org/10.1155/2022/5899199

Research Article

Fill-In and Boiling Transition Characteristics during the Liquid Oxygen Chill-Down Process in a Vertical Exit-Contracted Pipe

Jiaqi Zhang, Ke Wang, and Lanwei Chen

Science and Technology on Scramjet Laboratory, College of Aerospace Science and Engineering, National University of Defense Technology, Changsha 410073, China

Correspondence should be addressed to Jiaqi Zhang; amatyer_a@hotmail.com

Received 2 July 2022; Accepted 27 July 2022; Published 23 August 2022

Academic Editor: Yiheng Tong

Liquid oxygen chill-down in a vertical exit-contracted pipe was investigated experimentally. The wall temperatures were recorded in detail to describe the filling and chill-down process of the experimental section. Two quenching fronts, the exit one and the inlet one, were detected, and their propagations were found. Results show that the chill-down process is controlled mainly by the formation and propagation of quenching front, which are determined by the pressure level. With the increase of pressure, the roles of both propagation of quenching front and inlet quenching front undergo decreasing. On the vertical section, the effect of circumferential position was discussed in detail and the dominant point was identified, which determines the boiling transition time of the dominated points on the current cross-section. Based on the experimental data, two correlations were suggested for dominant point and dominated points, respectively, to predict heat flux on Leidenfrost, heat transfer coefficient on Leidenfrost, and critical heat flux. One equation was approved to predict heat transfer coefficient on critical heat flux point for both sorts of points. All of these correlations could produce reliable predictions.

1. Introduction

Liquid oxygen (LO_2) and liquid methane (LCH_4) are characterized by low-cost, nontoxic, high performance compared to hypergolic propellants, and both of them could be produced on Mars [1, 2]. In this way, a number of projects have been put forward to support future exploration missions using this cryogenic propellant combination [3]. Systematical demonstrations indicated that for space propulsion using this combination, the primary technical risks included the cryogenic fluid management (CFM) and the low-pressure engine technology [4–6].

A number of studies have been put forward to improve the technology readiness level (TRL) for CFM system [3]. For this system, cryogenic fluid could be the liquid phase when the container or pipe are cooled to the liquid temperature. In this way, cryogenic chill-down in the transportation pipe is one of the basic processes here, especially for refueling and transportation of the cryogenic propellants [7]. With the cryogenic fluid first flowing into the pipe with room temperature, flash vaporization would happen in the pipe. Figure 1 gives a typical process of cryogenic chill-down. With the pipe temperature decreasing, fluid pattern in the pipe undergoes film boiling, transition boiling, nucleate boiling, and single phase in sequence. These 4 flow patterns are divided by 3 boiling transition points, Leidenfrost (LFP), critical heat flux (CHF), and onset of nucleate boiling (ONB) [8].

A number of studies have been put forward to investigate the cryogenic chill-down in the transport pipeline. A series of visual studies have been put forward [9, 10], and based on them, a series of phenomenological models have been set up to model the cryogenic chill-down process [11, 12]. For setting up more reliable model, recently, a number of experimental studies have been performed [13–21] to correlate the heat transfer coefficients for various boiling patterns and boiling transition points (LFP, CHF). It is believed that in the current stage, correlations approved by Darr et al. [15, 16] could obtain general

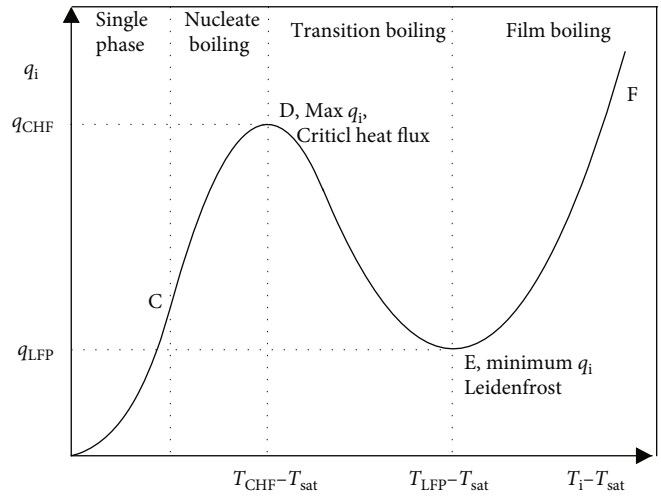

Figure 1: Typical boiling curve and flow patterns for chill-down process.

applications for transport pipe. Based on the improvement on models, a couple of reliable numerical results have been obtained [22, 23].

For low-pressure cryogenic engine, the primary technical difficulty is the instable combustion associate with the two-phase injection produced by cryogenic chill-down [24]. As Figure 2 [25] shows, taking LO_2 for example, before start-up, components upstream of point G would be chilled completely by LO_2 outflow through the prechilling valve. During the start-up process, liquid propellant flows into the components downstream of point G in ambient temperature, which produces two-phase injection and instable combustion in the combustion chamber of the engine [24]. Basically, this phenomenon could be avoided by chilling the components downstream point G before start-up [26]. However, in most cases, the feasibility of this process is determined mainly by the engine procedure. Furthermore, it has been found that two-phase injection could not be avoided even after start-up process [27].

Cryogenic chill-down in low-pressure engine is characterized by the components downstream point G, with a flow contraction on the exit, known as injector, which could be reduced to an exit-contracted pipeline as Figure 3 shows [8, 28]. This is much different from that in transportation pipe taking CFM system as the investigation background, without any flow contraction on the exit.

In the previous studies, cryogenic chill-down in exit-contracted pipe has not been distinguished from cryogenic chill-down in transport pipe. A series of pioneered experimental studies on cryogenic chill-down in the horizontal exit-contracted pipe have been performed by the present authors [8, 28, 29]. Chill-down process was discussed, and boiling transition points were correlated. It has been found that boiling transition points could be well correlated by formats from pool boiling for the exit-contracted pipe, rather than formats from flow boiling from transport pipe [8]. However, the latest study showed that the quenching front seems to be formed in the center length in the horizontal exit-contracted pipe, then propagates to the both ends of the pipe during the chill-down process. In addition, gravity or the circumferential position (bottom, top, or side) plays significant role [29]. This induces extra difficulty to model the heat transfer and transition boiling points in exit-contracted pipe, which is much different from that in transport pipe [16].

It has been concerned that the effects of both gravity and propagation of the quenching front play significant roles in the previous study that [29]. In the present study, for excluding the effect of gravity, vertical pipe would be applied instead of horizontal pipe. In this way, experimental study would be performed to investigate the chill-down process by a constant flow rate of LO_2 in a vertical exit-contracted pipe. A series of tests with the same flow rate and various pressure in the pipe would be performed. Chill-down process would be tracked, by which the propagation of quenching front would be investigated. Based on these data, boiling transition points would be discussed, and q_i and h_i on these points would be correlated for vertical pipe section.

2. Experimental Methodology

2.1. Experimental Platform. Figure 4 gives the experimental platform applied in the present study. It is the LO_2 branch of a typical test platform for cryogenic engine. Compared to the previous one applied in the previous studies [8, 28], the present platform has been upgraded, where the previous 100 L/5.5 MPa LO_2 tank is replaced by a 500 L/10 MPa one. Other parts of the present platform are the same with the previous ones. As shown in the figure, flow rate of the fluid is controlled by the Venturi nozzle.

2.2. Experimental Section and Measurement Approach. Figure 5 gives the experimental section in detail. The shape of experimental section applied could be drawn in Figure 5(a), which also indicates the necessary sensors measuring the pressure and temperature of the fluid. As shown in the figure, a pressure sensor (PT301) and a temperature sensor (PT100) are set up on the experimental section to measure the pressure and temperature of the fluid,

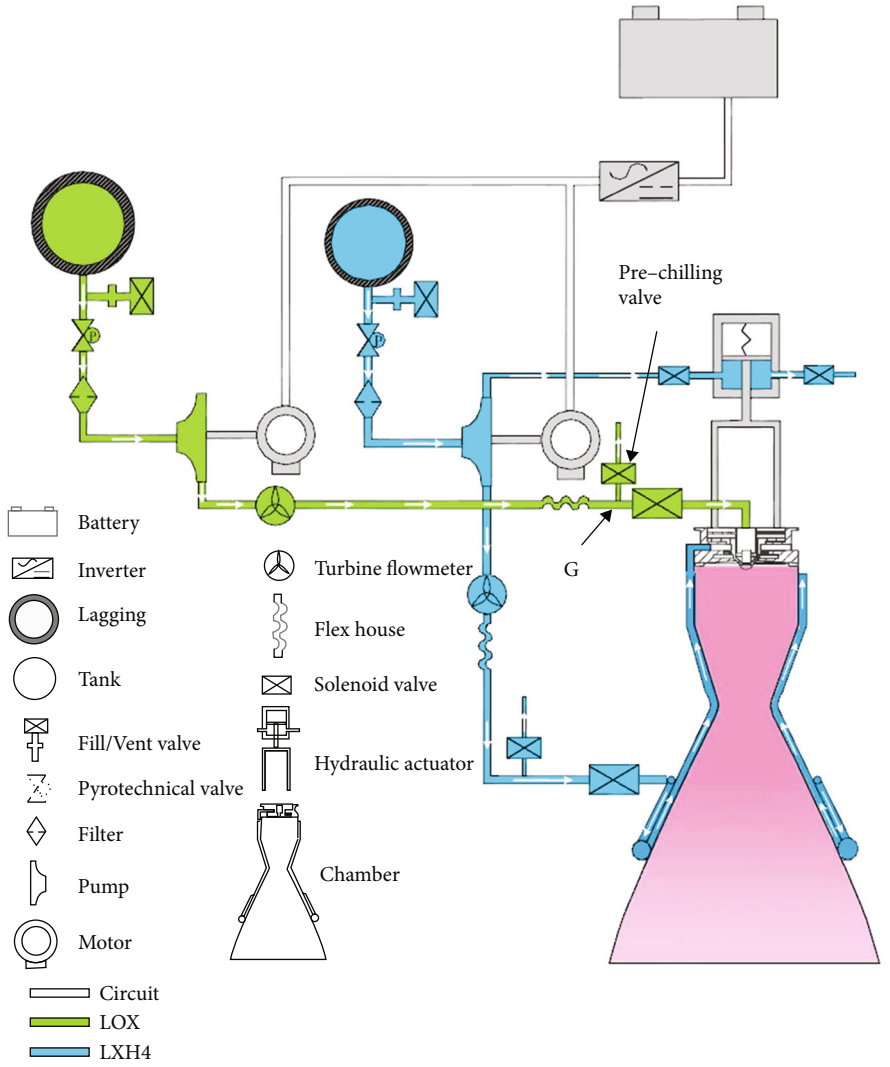

Figure 2: Sketch of a typical low-pressure cryogenic engine [25].

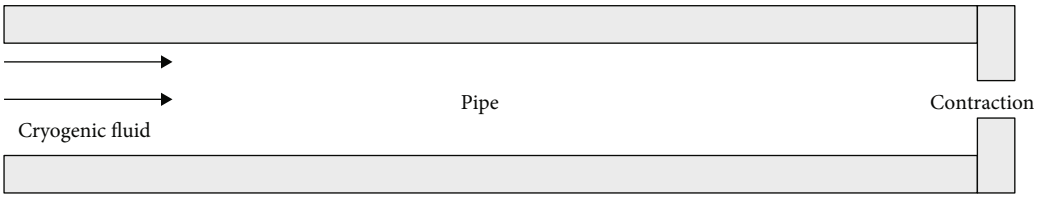

Figure 3: Pipe with a contraction on the exit.

respectively, in the section. 13 T_o sensors (T-type thermocouples) were welded on the outer surface of the experimental section, and they were distributed on 5 cross-sections (various L_{se}) as Figure 5(a) shows. Figure 5(b) gives the cross-section (vertical) on $L_{se} = 1.55$ m, where the 2 sensors, denoted by 1.55-1 and 1.55-2, were welded on the bottom and south-side of the pipe, respectively. The cross-section (horizontal) for other L_{se} could be shown in Figure 5(c), which shows for every section, 3 sensors were set up on the west, south, and east of the pipe in turn (2 sensors on the west and south for $L_{se} = 0.3$ m, denoted by 0.3-1 and 0.3-2). T_o data were recorded by temperature scanner (EX32A). All of the above sensors are with the scan rate of 1000 Hz.

2.3. Other Conditions. For minimizing the potential deviations including nitrogen solution in LO_2 and flow rate oscillations, the test process were well designed and illustrated as shown in reference [1], which would not be repeated here.

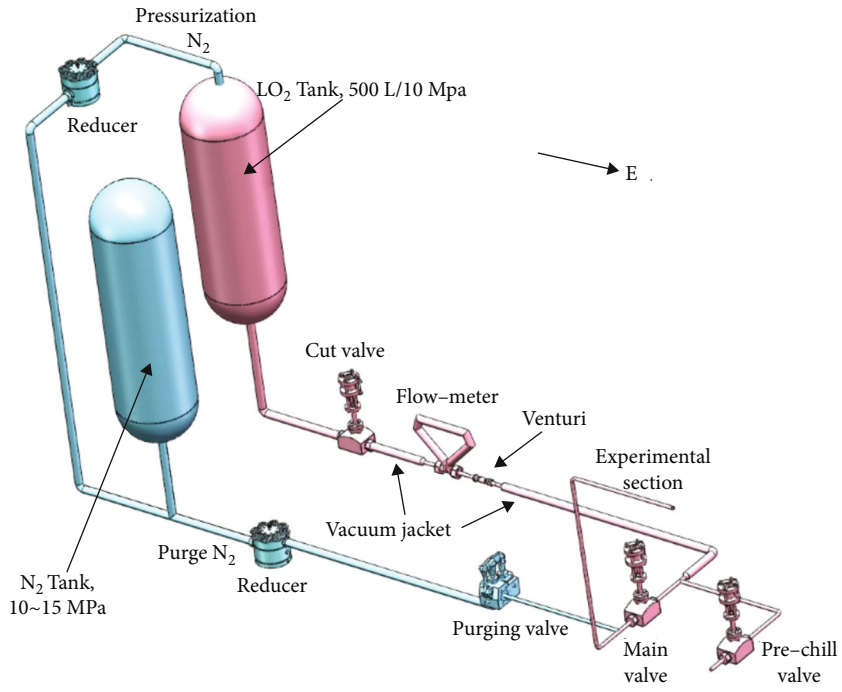

Figure 4: Experimental system of the present study.

3. Experimental Results

3.1. Basic Results. Four tests were performed, and related conditions and results could be listed in Table 1. It shows that the present series of tests are all with the similar flow rate and various A_{inj}. With the decrease of A_{inj} (Exp. 1~4), pressure in the experimental section shows the increasing manner. This indicates that the P_{ss} range is from 0.328 to 1.325 MPa.

3.2. Data Processing and Boiling Transition Points. Parameters in the pipe as well as T_o data were measured for all of the four tests. By processing T_o data, T_i and q_i were obtained because most discussions next would be based on these 2 parameters. Here, T_i would be determined according to reference [30], and q_i would be obtained by numerical methods introduced in the previous studies [28], which would not be repeated here anymore.

Based on T_i and q_i data, boiling curves could be drawn. In this way, boiling transition points, LFP, and CHF could be determined as well. These two points could be identified in the boiling curve easily, which indicate the minimum q_i point and maximum q_i point, respectively.

3.3. Uncertainty. The present study focuses on the comparison between experimental values and predicted values for T_{LFP}, q_{LFP}, T_{CHF}, and q_{CHF}. The experimental values depend mainly on the T_o measurement, physical properties as well as the geometric parameter of the pipe. On the other hand, as shown in the correlations, the predicted values depend mainly on the measured pressure and geometric parameter of the pipe. These factors could be shown in Table 2. Furthermore, the respective mean absolute errors (MAE) can be defined as Equation (1) shows [31].

$$\text{MAE} = \frac{1}{N}\sum \frac{\left|V_{exp} - V_{pre}\right|}{V_{exp}} \times 100\%. \quad (1)$$

3.4. Basic Chill-Down Process. Figure 6 shows all of the T_i curves as well as T_p, T_{sat}, and P_p curves to show the chill-down process for Exp. 1. As shown in the figure, during the chill-down process, T_p, T_{sat}, and P_p curves show the similar manner with the curves recorded in the previous studies [8, 28]. It also shows that a typical T_i curve is composed by three sequent phases as follows.

(1) Phase I: the initial linear decrease phase. In this phase, T_i decreases in a linear manner, which indicates the inner flow is on the film boiling. LFP, the transition point between film boiling and transition boiling, could be seen as the transition point between phases I and II as well

(2) Phase II: the sudden decrease followed by phase I. This phase is with the shortest period, in which T_i decreases dramatically. This phase involves both transition boiling section and nucleate boiling section, and CHF, the transition point between transition boiling and nucleate boiling, sometimes would be seen as the central point of it

(3) Phase III: the gradual decrease followed by phase II. In this phase, T_i decreases gradually, which indicates the inner flow is the single-phase flow. As shown in Figure 1, the transition point between phase II and phase III is denoted as ONB, which always indicates the end of chill-down

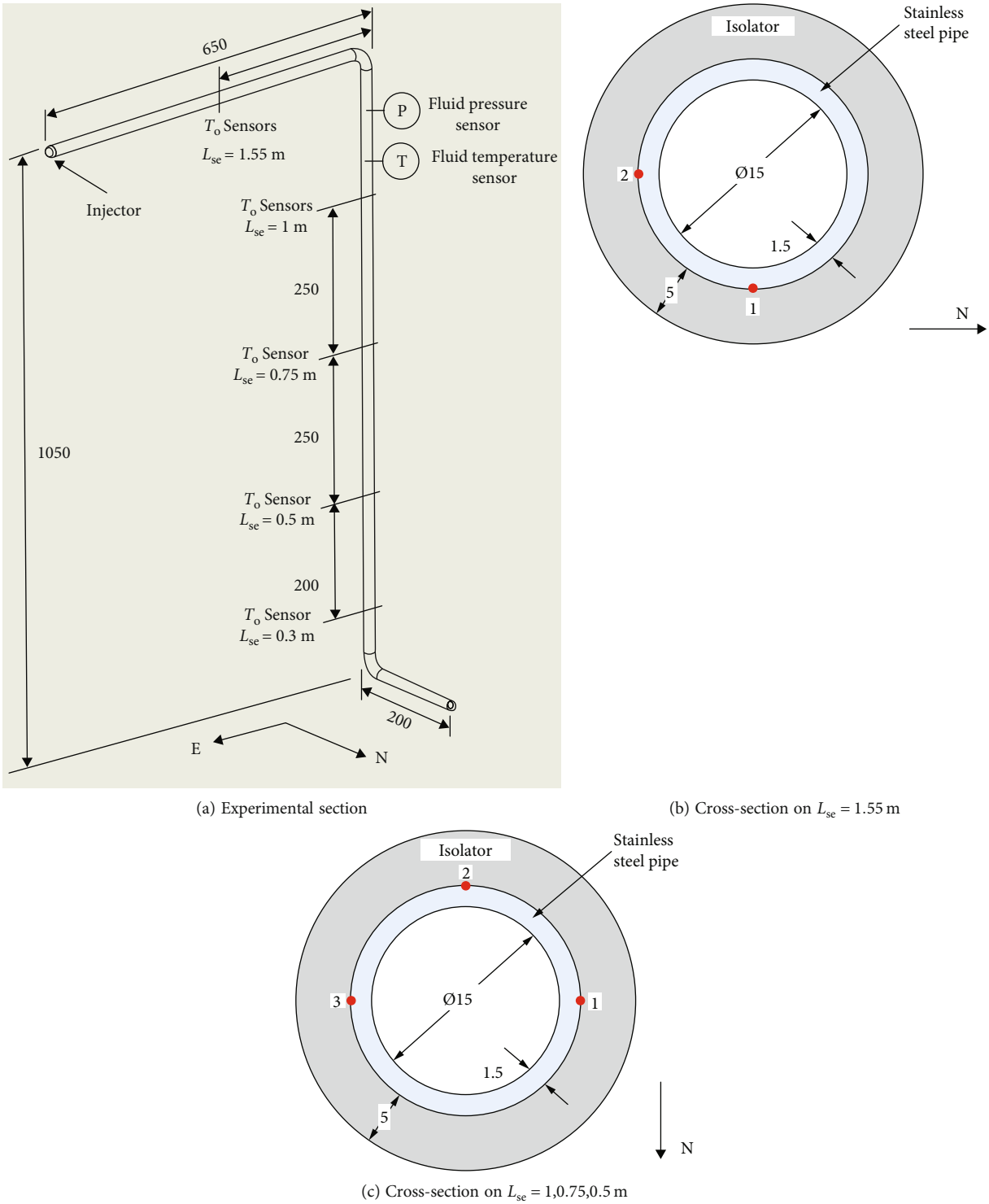

Figure 5: Details on the experimental section, unit: mm.

As shown in Figure 6, for Exp. 1, T_i on L_{se} = 1.55 m decreases at first, followed by L_{se} = 0.3 m, 1 m, 0.75 m, and 0.5 m in turn. Similarly, LFP happens in L_{se} = 1.55 m at first, followed by L_{se} = 0.3 m, 1 m, 0.75 m, and 0.5 m in turn. This indicates that two quenching fronts (QF) are formed on the exit and inlet of the experimental section independently. In the current stage, the exact positions of them could not be decided yet. However, based on the current information, the characteristics of QF formation and propagation could be approved.

It is evident that the QF formed near the exit propagates backward, from somewhere downstream of L_{se} = 1.55 m to the inlet section. It gets to L_{se} = 1.55 m, 1 m, 0.75 m, and 0.5 m in turn and produces boiling transitions on these points. On the other hand, the inlet QF propagates forward from the inlet section to the exit, and it gets to L_{se} = 0.3 m

Table 1: Experimental conditions and results.

Parameters	Exp. 1	Exp. 2	Exp. 3	Exp. 4
Injector type	Orifice	Pintle	Pintle	Orifice
A_{inj} (mm)	110.6	67.2	33	12
$\dot{m}$ (kg/s, start)	0.44	0.435	0.429	0.417
$\dot{m}$ (kg/s, end)	0.45	0.444	0.438	0.426
G (kg/(m^2•s), end)	2546	2513	2478	2411
Re (end)	259192	270824	319074	329295
T_p (K, end)	101.5	104	112	115
$T_{sat} - T_p$ (K, subcooling, end)	1.65	2.06	3.3	9.64
P_{peak} (MPa, start)	0.586	0.843	1.678	3.049
P_{ss} (MPa, end)	0.328	0.41	0.77	1.325

Table 2: Summary of the uncertainties.

Parameters	Uncertainty
Fluid pressure (%)	0.5
Fluid temperature (K)	1
Outer wall temperature (K)	1
Pipe D_i and D_o (mm)	0.01
Mass flow rate (%)	1
T_o (K)	1
T_i (K)	2
q_i (%)	5

and produces boiling transition here. It has to be noted that QFs get to $L_{se} = 1.55$ m and $L_{se} = 0.3$ m almost simultaneously at 10 s. However, after that, it seems like that the inlet QF does not propagate forward, and the vertical section is chilled by the exit QF.

As shown in Figure 7, for Exp. 2, T_i on $L_{se} = 1.55$ m decreases at first, followed by $L_{se} = 1$ m, 0.75 m, 0.3 m, and 0.5 m in turn, and LFP shows the similar manner. However, as shown in Figure 8 and Table 3, for Exp. 3, T_i on $L_{se} = 1.55$ m decreases at first, followed by $L_{se} = 1$ m, 0.75 m, 0.5 m, and 0.3 m in turn, and LFP shows the similar manner. However, as shown in Figure 9 and Table 3, for Exp. 4, T_i on $L_{se} = 1.55$ m decreases at first. After that, T_i values on $L_{se} = 1$ m, 0.75 m, and 0.5 m decrease with the similar slope, which are obvious prior to $L_{se} = 0.3$ m. This indicates that QF on $L_{se} = 0.3$ m happens at first for Exp. 1, at the fourth place for Exp. 2, and at last for Exp. 3 and Exp. 4.

3.5. Mechanisms of the Chill-Down Process and the Quenching Front Propagation. As discussed above, especially Table 3, obviously, pressure plays significant role on the chill-down process. In another word, chill-down process is controlled by the formation and propagation of QFs, which is determined by the pressure level. In this way, the key point here is how to explain the relationship between pressure and the formation and propagation of QFs.

Apparently, these relationships are obvious. For Exp. 1 and Exp. 2 (low pressure relatively), the propagation of the exit QF determines the LFP of the experimental section for $L_{se} = 0.5$ m and its downstream, and LFP on $L_{se} = 0.3$ m are likely to be controlled by the inlet QF. For Exp. 3 (medium pressure relatively), it seems like that LFPs on all of the L_{se} points measured are controlled by the backward propagation of the exit QF. However, for Exp. 4 (high pressure relatively), the exit QF gets to $L_{se} = 1.55$ m. After that, QFs form almost simultaneously on all of the measured L_{se} points except $L_{se} = 0.3$ m; then, one of the QF (formed around $L_{se} = 0.5$ m) propagates to form LFP on $L_{se} = 0.3$ m.

In this way, the overall chill-down process in the experimental section could be described. For low-pressure cases, as the LO_2 flows into the experimental section, it produces intensive evaporation, and liquid core surrounded by the vapor flows to the exit. Because of the contraction on the pipe exit, outflow of the vapor-liquid mixture would be chocked to enhance the system pressure. Simultaneously, because the flow contraction is with high temperature, only vapor could flow out, which produces the liquid accumulation around the injector. As a result of liquid accumulation, heat transfer is enhanced, and QF is formed here at first. After that, QF moves from the exit of the pipe to the upstream of the experimental section. This process is similar with that discussion before [29]. For medium pressure cases, this process does not show obvious change. The only difference is that the duration is shortened by the enhancement of h_{FB} produced by enhanced pressure. For high pressure relatively, the propagation of exit QF also plays significant role on the section near the exit. However, in most vertical section, QFs are formed almost simultaneously for all of the three L_{se}. This indicates that for this case, the role of QF propagation decreases.

On the other hand, simultaneously, the inlet QF could be formed at the inlet of the experimental section. It plays significant role for low-pressure cases and decreasing roles with the increase of pressure. In addition, another possibility is the effects of inlet QF would be reduced by the corner of the experimental section near the inlet.

Traditionally, QF propagates from the inlet to the outlet of the experimental section for transport pipe, and most correlations are independent on this characteristic [7]. However, recently, experimental studies on exit-contracted pipe show that the quenching front forms in the central length of the horizontal pipe [29]. In the present study, both inlet QF and outlet QF are found. This is different from the previous studies, in the transport pipe [7] or horizontal exit-contracted pipe [29].

4. Film Boiling Heat Transfer and the Leidenfrost Point

In the present section, film boiling heat transfer, liquid rewetting, and LFP would be discussed for $L_{se} = 0.5$, 0.75 and 1 m. This is primary because these cross-sections are set on the vertical section, and the LFPs of them are primary controlled by the exit QF, at least for lower and medium pressure cases.

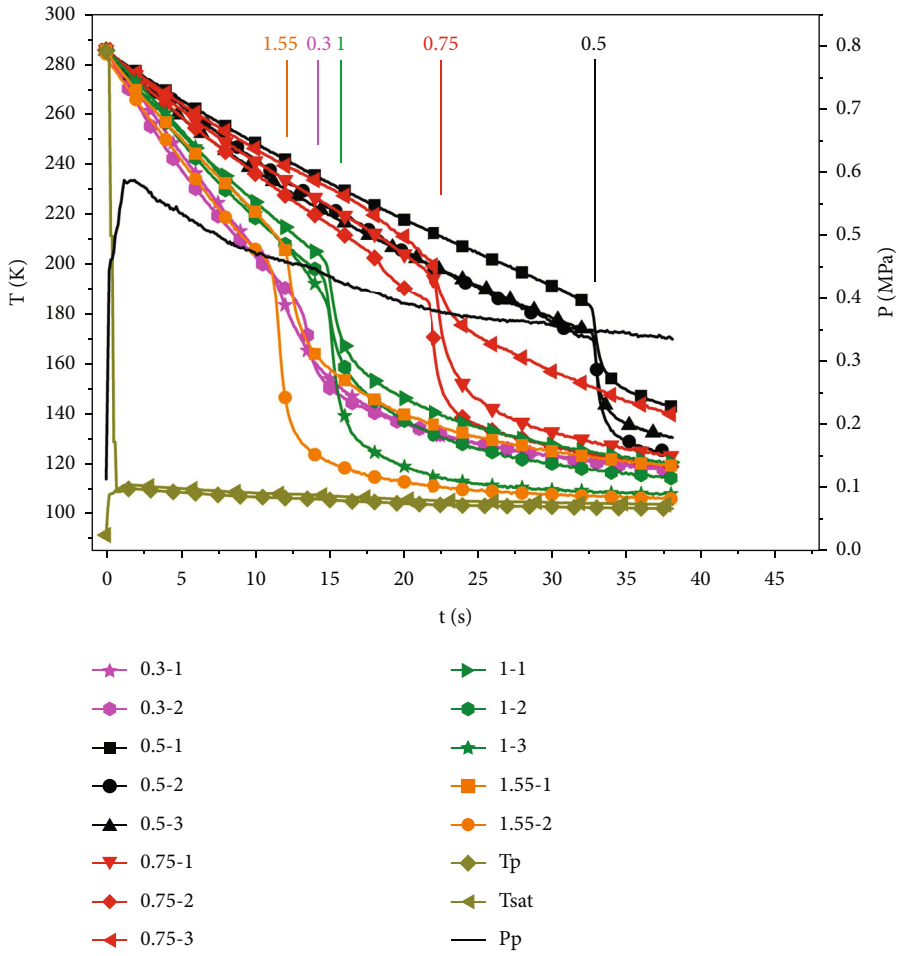

Figure 6: Tested data curves for Exp. 1 (0.45 kg/s, $P_{ss} = 0.328$ MPa).

4.1. Basic Effect of A_{inj}. The experimental ΔT_{LFP}, q_{LFP}, and h_{LFP} versus A_{inj} could be shown in Figure 10–12, respectively. It shows that, basically, with the decrease of A_{inj}, both q_{LFP} and h_{LFP} show the increasing manner (except some individual cases). On the other hand, with the decrease of A_{inj}, approximately, ΔT_{LFP} shows the increase manner for $L_{se} = 0.5$ m, the decrease manner for $L_{se} = 0.75$ m, and increase-decrease manner for $L_{se} = 1$ m. This is similar with those indicated in reference [29].

4.2. Evaluation of the Previous Correlations. Leidenfrost point (LFP), on which the liquid rewets the pipe wall, is known as the transition point from film boiling to transition boiling. This point is always identified as the point with the minimum heat flux. Historically, based on the flow instability theories, Zuber et al. [32] improved the basic correlation on q_{LFP} as shown in Equation (2) ($C_1 = 0.09$). After that, Berenson [33] approved Equation (3) ($C_2 = 0.425$) to evaluate h_{FB}, the heat transfer coefficient on film boiling, and suggested Equation (4) ($C_{LFP} = 0.127$) on LFP to evaluate ΔT_{LFP} based on basic heat transfer equation, Equation (6). After that, most correlations on q_{LFP} and ΔT_{LFP} for both pool boiling and flow boiling were based on these 2 equations. In the previous studies, ΔT_{LFP} and q_{LFP} were tried to be correlated. In this way, Equation (4) and Equation (2) were applied to predict ΔT_{LFP} and q_{LFP}, respectively, for horizontal exit-contracted pipe [8, 29].

$$q_{LFP} = C_1 \rho_v H_{vl} \left(\frac{\sigma_{vl} g (\rho_l - \rho_v)}{(\rho_l + \rho_v)^2} \right)^{0.25}, \tag{2}$$

$$h_{FB} = C_2 \left[\frac{k_v^3 H_{vl} \rho_v g (\rho_l - \rho_v)}{\mu_v \Delta T_i \sqrt{\sigma_{vl} / g (\rho_l - \rho_v)}} \right]^{0.25}, \tag{3}$$

$$\Delta T_{LFP} = T_{LFP} - T_{sat} = C_{LFP} \cdot E_{LFP}, \tag{4}$$

$$E_{LFP} = \frac{\rho_v H_{vl}}{k_v} \left(\frac{g (\rho_l - \rho_v)}{\rho_l + \rho_v} \right)^{2/3} \left(\frac{\sigma_{vl}}{g (\rho_l - \rho_v)} \right)^{1/2} \left(\frac{\mu_v}{g (\rho_l - \rho_v)} \right)^{1/3}, \tag{5}$$

$$q_i = h_i \Delta T_i. \tag{6}$$

According to Equation (4), in the present study, for vertical experimental section, ΔT_{LFP} could be plotted versus E_{LFP} in Figure 13, where C_{LFP} could be correlated to be 0.0576 and produces the MAE of 16.62%. As shown in the

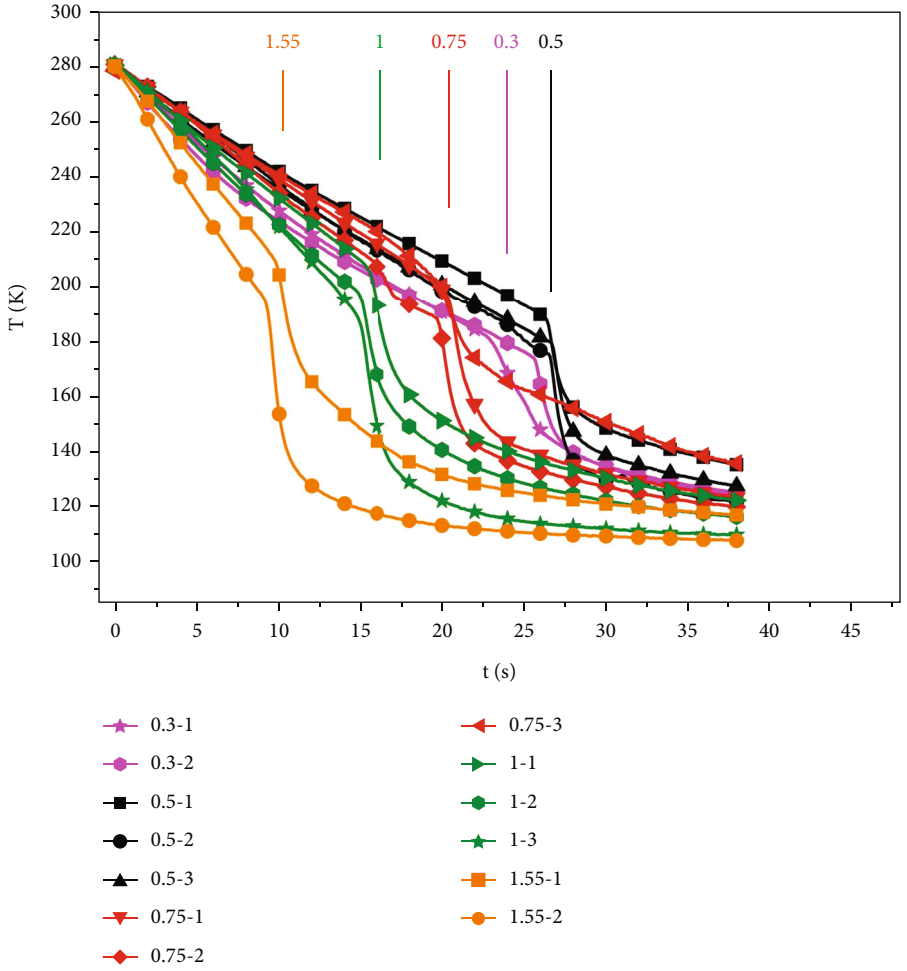

Figure 7: Tested data curves for Exp. 2 (0.444 kg/s, $P_{ss} = 0.41$ MPa).

figure, the point distribution and constant C_{LFP} do not show significant differences from the previous studies [29]. It shows that with the increase of A_{inj}, ΔT_{LFP} shows the overall increasing manner for $L_{se} = 0.5$ m and overall decreasing manner for other L_{se}. This indicates the similar difficulties on correlation, which has been discussed in the previous studies in horizontal pipes [29].

On the other hand, Zuber's correlation, Equation (2), indicates that on LFP, vapor was not produced rapidly enough to lift the interface as rapidly as it would normally collapse [34]. In this way, q_{LFP} in the present study could be correlated by this equation as shown in Figure 14, where the constant C_1 and MAE could be listed in Table 4. Generally speaking, as shown in Equation (2), the effects of fluid properties could be represented by the items in the abscissa of Figure 14, and the effects of circumferential position and L_{se} could be represented by the variable parameter C_1, which has been correlated for every point. Obviously, it is not a general correlation. However, in the current stage, this equation is important to set up the basic outline for the following investigations.

As shown in Figure 14, basically, Equation (2) could produce reliable predictions on q_{LFP} for $L_{se} = 0.5$ and 0.75 m relatively. However, for $L_{se} = 1$ m, with the increase of $\rho_v H_{vl}(\sigma_{vl} g(\rho_l - \rho_v)/(\rho_l + \rho_v)^2)^{0.25}$, q_{LFP} shows the decreasing-increasing manner. Thus, from the view of point of correlation, Equation (2) could be used to produce q_{LFP} for $L_{se} = 1$ m only on higher pressure (e.g., $P_{ss} \geq 0.4$ MPa). In this way, C_1 items listed in Table 4 for $L_{se} = 1$ m were correlated for Exp. 2~4.

4.3. Correlations on h_{LFP}. By the present set of data, h_{LFP} could be correlated by Equation (3) as shown in Figure 15, where the constant C_2 could be listed in Table 4. Basically, with the increase of pressure, the 2nd item of the right side of Equation (3) keeps increasing constantly, which is consistent to the experimental h_{LFP} data.

4.4. Primary Effect Factors. According to Carbajo [35], liquid rewetting involves the effects of pressure, liquid subcooling, liquid and solid properties, surface conditions, and flow rate. However, in the present study, throughout all of the tests, only pressure shows the obvious variations. On the other

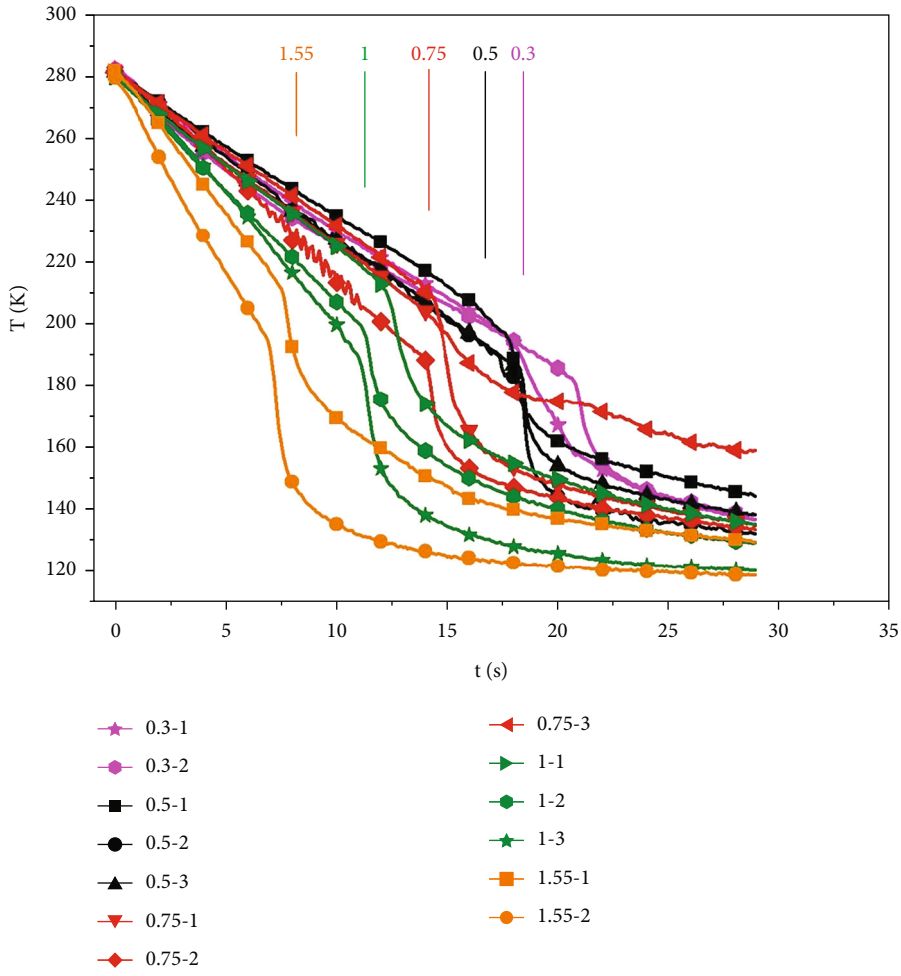

Figure 8: Tested data curves for Exp. 3 (0.438 kg/s, P_{ss} = 0.77 MPa).

Table 3: Statistical t_{LFP}/t_{CHF} data (unit: s).

Position	Exp. 1	Exp. 2	Exp. 3	Exp. 4
0.3-1	10/11.9	22/23.6	13/18.9	8/11.7
0.3-2	11/13.7	22/25.9	16/21.3	9/13
0.5-1	29/33.1	23/26.7	12/18.3	6/9.1
0.5-2	28/33.2	22/26.8	12/18.7	5/9.5
0.5-3	30/33.2	25/27	12/18.7	5/8.7
0.75-1	18/22.6	17/20.7	10/15.2	6/9.6
0.75-2	15/22.3	14/20.1	10/14.5	6/8.8
0.75-3	16/22.4	15/20.2	10/14.8	6/9.5
1-1	14/15.4	13/16	8/13	6/9.2
1-2	14/15.2	14/15.3	8/11.7	6/8
1-3	11/15.4	13/15.3	8/11.7	5/8
1.55-1	10/12.6	8/10.2	6/8	4/5.1
1.55-2	10/11.8	8/9.6	5/7.5	4/4.7

hand, L_{se} and circumferential positions are obviously different for these points. In this way, the effects of pressure, L_{se}, and circumferential positions would be discussed in the present section.

4.4.1. The Effects of A_{inj} or Pressure. The present series of tests are with the same flow rate. Thus, the effects of A_{inj} in the present study indicates the effects of pressure only. On the film boiling section, with the decrease of A_{inj} (increase of pressure), h_{FB} keeps increasing because δ_{FB} keeps almost constant and k_v keeps increasing as shown in Equation (7) [29].

$$h_{FB} = \frac{k_v}{\delta_{FB}}. \tag{7}$$

In this way, with the increase of A_{inj}, the slope of T_i decreasing increases for every point, and chill-down period (t_{LFP}) would be shortened as well. As a result, both heat flux and heat transfer coefficient would be enhanced on film boiling section, which produces the overall increasing q_{LFP} and h_{LFP} for every point.

These principles are very similar with those tendencies in horizontal exit-contracted pipe [29].

4.4.2. The Effects of L_{se}. Traditionally, h_{LFP} decreases with the increase of L_{se} according to the existing correlations [7]. However, in the present study, experimental data do not

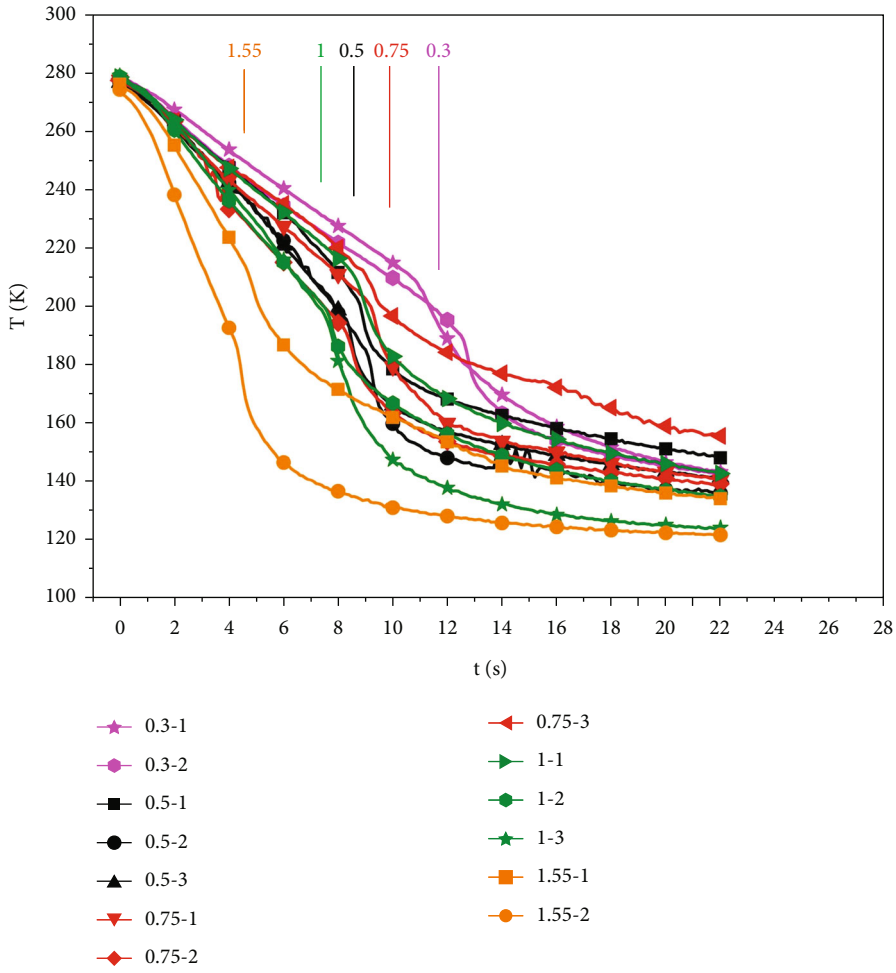

Figure 9: Tested data curves for Exp. 4 (0.426 kg/s, P_{ss} = 1.325 MPa).

show the similar tendency. Comparison between Figures 14 and 15 shows that, for a certain test, both q_{LFP} and h_{LFP} increase with the increase of L_{se}, which is contrary to that in transport pipe [7]. Comparison among transport pipe [7], horizontal exit-contracted pipe [29], and vertical exit-contracted pipe indicates that the effects of L_{se} traditionally concerned are essentially more like the effects of L_{qf}, distance from the present point to the QF formation point. In this way, experimental results in reference [29] and in the present study could be explained well. Thus, it is necessary to denote that from the view of point of pipe length, L_{qf} plays the significant role on LFP instead of L_{se}.

In general, for a certain test, along the directions of QF propagation, t_{LFP} shows the increasing manner, compared to that q_{LFP} and h_{LFP} show the decreasing manner. This characteristic plays significant roles on the LFP. This indicates the basic principle, longer L_{qf} is corresponding to greater t_{LFP}, lower q_{LFP} and h_{LFP}. This principle is always the case independent on L_{se} and the dominant QF, even for L_{se} = 0.3 m, on which even the LFP is controlled by various QF.

For a certain L_{se}, with the increase of A_{inj}, t_{LFP} shows the decreasing manner, and q_{LFP} and h_{LFP} show the increasing manner. This indicates that with the increase of pressure, both h_{FB} and M (magnitude of instable waves) undergo corresponding increase. According to results in horizontal exit-contracted pipe [29], LFP is controlled by the competition between heat transfer and the increase of M. However, according to the present study, QF propagation also plays a significant role on. In the present study, for Exp. 1~3, QF propagation could be well tracked according to the experimental data, which indicates that the latter one is the dominant factor. However, for Exp. 4, LFP happens almost simultaneously on L_{se} = 0.5, 0.75, and 1 m, which indicates that the former is the dominant factor in this case.

Another key point is where is the QFs formed. In the present study, both inlet QF and exit QF are identified. Analysis indicates that QF formation is controlled by the fill process of the cryogenic fluid in the exit-contracted pipe.

4.4.3. The Effects of Circumferential Position. As shown in Table 3, for every L_{se}, t_{LFP} values for circumferential position (1, West; 2, South; 3, East) are quite similar to each other. This indicates the propagation of QF circumferentially also plays significant role. This is similar with those in horizontal exit-contracted pipe [29]. However, traditionally,

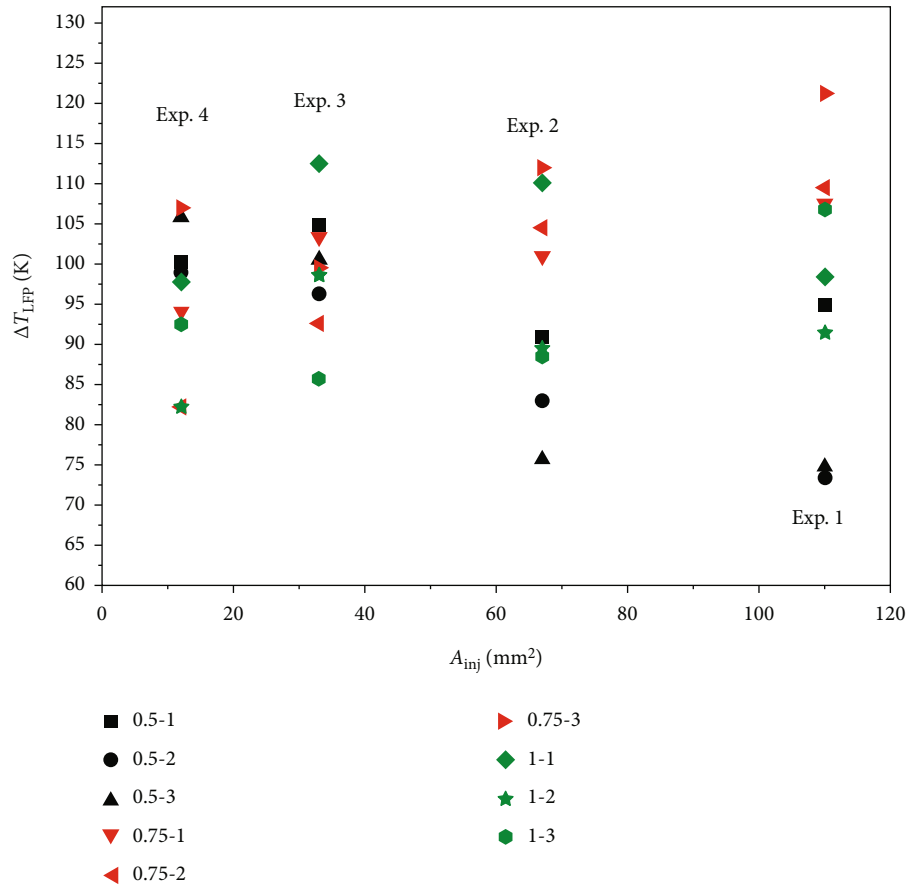

Figure 10: Experimental ΔT_{LFP} versus A_{inj}.

circumferential position plays ignorable role in the vertical transport pipe [7]. In the present study, vertical section (L_{se} = 1, 0.75, and 0.5 m), as shown in Table 4, could produce around 50% variation on h_{LFP} and q_{LFP} and q_{CHF} for L_{se} = 1 and 0.75 m and 30% for L_{se} = 0.5 m.

In this way, for a certain L_{se}, h_{FB} always dominates the decrease of T_i on points 1~3. After that, once one of them gets to LFP, boiling transitions would happen immediately on other two points, which produces the h_{FB} at that time as h_{LFP}. In another word, on the same L_{se} cross-section, various points are with the similar t_{LFP}.

In this way, three points, 0.5-2, 0.75-2, and 1-3 are the dominant points for L_{se} = 0.5, 0.75, and 1 m, respectively, and determines the t_{LFP} point on the present section in the present study. For other points (dominated points), during the chill-down process, q_i and T_i keep decreasing, and h_{FB} keeps increasing. Once LFP happens at t_{LFP} on the dominant point on the same section, liquid rewetting would happen on the dominated points. Thus, q_i, T_i, and h_{FB} at that time would be identified as q_{LFP}, T_{LFP}, and h_{LFP}.

This implies that on a certain L_{se} cross-section, the liquid rewetting mechanism for the dominant point is different from that for the dominated points. For the dominant point, liquid rewetting is more likely to be controlled by flow instability, which is similar with that on pool boiling or flow boiling. According to the series of data, this process is dominated by the QF propagation axially. However, for the dominated points, liquid rewetting is controlled by both the dominant point and the local heat transfer. This process is dominated by the QF propagation circumferentially.

The difference between the dominant point and dominated points could be also found in the horizontal exit-contracted pipe. Obviously, because of the gravity, the dominant point is the bottom point for horizontal pipe [29]. However, for the vertical pipe, the effect of gravity could be ignored. According to Carbajo [35], liquid rewetting involves the effects of pressure, liquid subcooling, liquid and solid properties, surface conditions, and flow rate. In this way, on the same L_{se} cross-section, this sort of difference between the dominant point and dominated points is probably caused by the inner surface conditions.

4.4.4. Summary on the Basic Effect Factors. As discussed above, the effects of pressure, L_{se}, and circumferential position could be summarized and concluded as follows.

(1) For a certain point, the increase of A_{inj} produces overall increasing q_{LFP} and h_{LFP} and deceasing t_{LFP}

(2) With the increase of L_{qf}, overall decreasing q_{LFP} and h_{LFP} and increasing t_{LFP} could be obtained

(3) Because of the propagation of QF circumferentially, on a certain L_{se} (cross-section), there are both dominant point and dominated points, which are

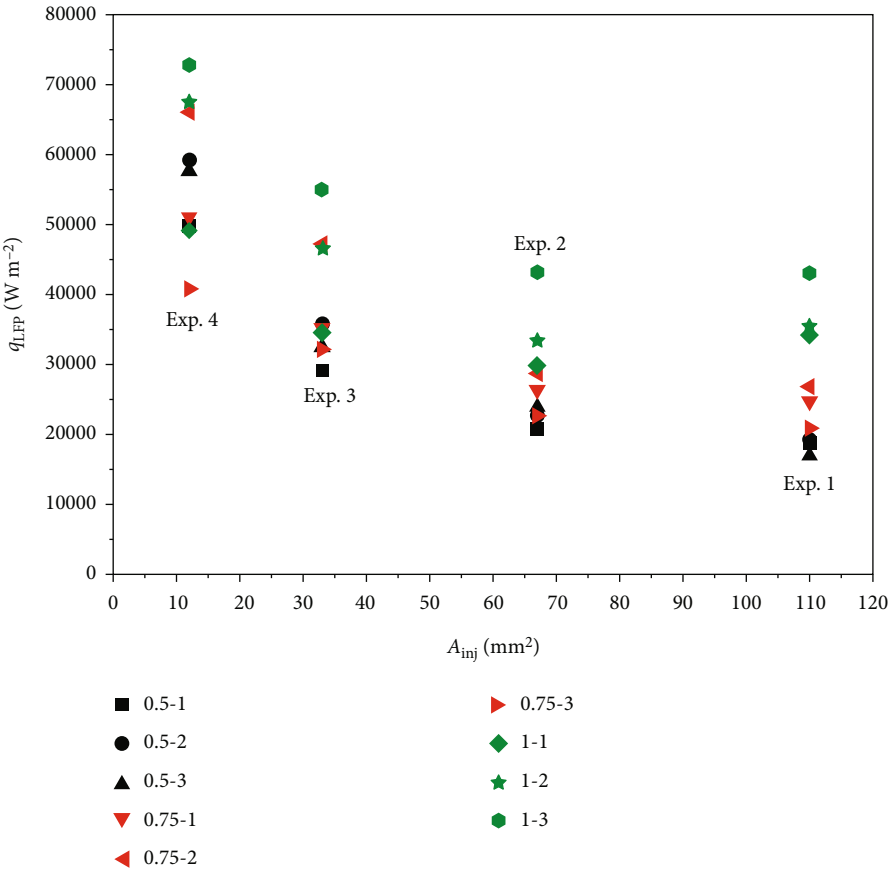

Figure 11: Experimental q_{LFP} versus A_{inj}.

controlled by flow instability and both dominant point and h_{FB} and, respectively. In the present study, 0.5-2, 0.75-2, and 1-3 are the dominant points for these sections, respectively.

4.5. Discussions

4.5.1. Correlations on the Dominant Points. From the view of point of correlation, all of these factors should be involved. For three dominant points, 0.5-2, 0.75-2, and 1-3, on which liquid rewetting is controlled by flow instability. According to Equation (2) and Table 4, C_1 for them are correlated to be 0.0643, 0.0748, and 0.086, respectively. It shows that C_1 increases linearly with the increase of L_{se} (decrease of L_{qf}). In this way, based on Equation (2), q_{LFP} on the dominant points for $L_{se} = 0.5$, 0.75, and 1 m could be correlated by Equation (8). This correlation could be approved for dominant points in vertical section.

$$q_{LFP} = (0.0425 + 0.0434L_{se})\rho_v H_{vl}\left(\frac{\sigma_{vl} g(\rho_l - \rho_v)}{(\rho_l + \rho_v)^2}\right)^{0.25}. \quad (8)$$

As discussed above, in the present study, q_{LFP} decreases with the decrease of L_{se} for $L_{se} = 0.5$ m and its downstream. In addition, on 1.55-2, the dominant point on $L_{se} = 1.55$ m, and the horizontal section, C_1 was correlated to be 0.1335, which has not been given above. This indicates the C_1 values along the QF propagation, from 0.1335 ($L_{se} = 1.55$ m) to 0.086 ($L_{se} = 1$ m), 0.0748 ($L_{se} = 0.75$ m), and finally, 0.0643 ($L_{se} = 0.5$ m). These series of values are consistent to the literature data, in which C_1 was correlated to be 0.09 [32] for room-temperature fluid in pool boiling. At first, the deviation of C_1 between the present study and reference [32] is mainly caused by the variations between the fill-in flow in the exit-contracted pipe and pool boiling. On the other hand, the decrease of C_1 along the reverse direction of the flow in the experimental section pipe indicates the special characteristics of flow in the exit-contracted pipe.

Similarly, according to Equation (3), C_2 for 0.5-2, 0.75-2, and 1-3 are correlated to be 0.573, 0.7139, and 0.8264, respectively. Similar with q_{LFP}, h_{LFP} on the dominant points for $L_{se} = 0.5$, 0.75, and 1 m could be correlated by Equation (9). This series of data is consistent to the literature data, in which C_2 was correlated to be 0.425 [33] for room-temperature fluid in pool boiling.

$$h_{FB} = (0.324 + 0.5068L_{se})\left[\frac{k_v^3 H_{vl}\rho_v g(\rho_l - \rho_v)}{\mu_v \Delta T_i \sqrt{\sigma_{vl}/g(\rho_l - \rho_v)}}\right]^{0.25}. \quad (9)$$

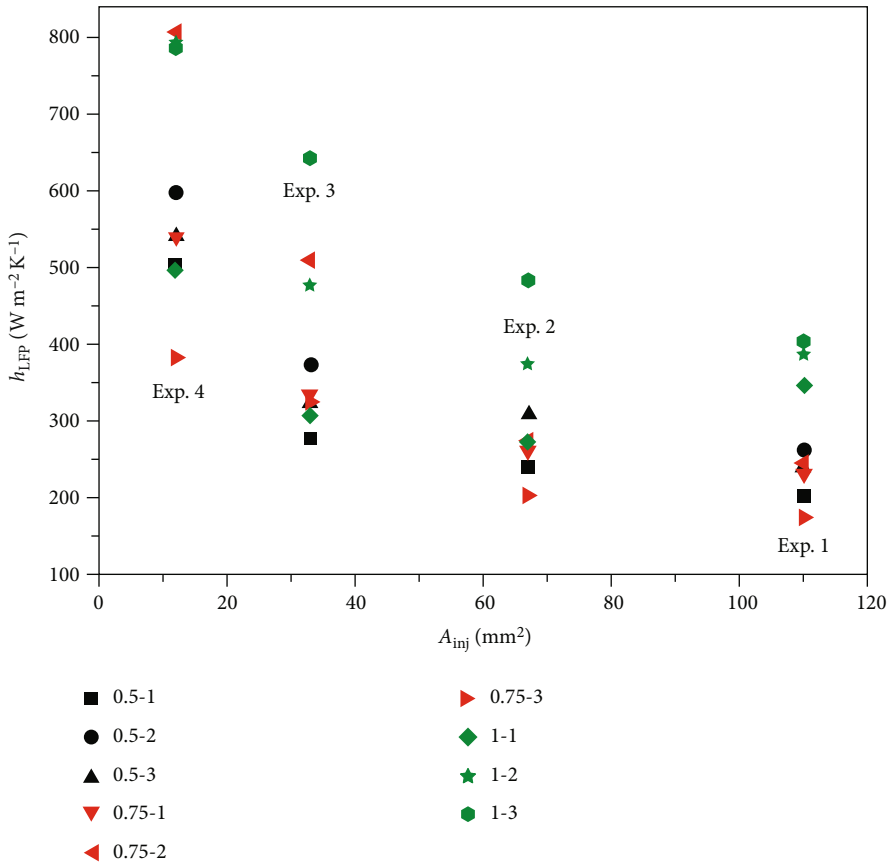

Figure 12: Experimental h_{LFP} versus A_{inj}.

Compared to the literature data from room-temperature fluid in pool boiling, dominant points in the vertical section are with lower q_{LFP}, lower ΔT_{LFP}, and higher h_{LFP}. Basically, this sort of differences is mainly caused by the variations on the system pressure and flow condition. On the other hand, the similarity on C_1 and C_2 between for exit-contracted pipe and pool boiling indicates that flow instability is the primary dominant factor, and L_{se} also plays a certain role for the dominant points on the present vertical pipe.

4.5.2. Correlations on the Dominated Points. For the dominated points, Equations (2) and (3) with constants listed in Table 4 could be suggested in the current stage. It has to be denoted that on this sort of points, liquid rewetting is not caused by local flow instability on this sort of points. On the contrary, the local instable wave has not been developed adequately. Result indicates that at t_{LFP}, liquid rewetting happens on the dominant point on the current cross-section. Almost simultaneously, all of this cross-section is rewetted by the liquid as a result of QF propagation circumferentially from the dominant point. In this way, on the dominated points, as a result of being rewetted, q_i, h_i, and T_i at t_{LFP} have to be denoted as parameters on LFP.

4.5.3. Correlation Approach and Correlation Formats. In the previous studies, q_{LFP} and ΔT_{LFP} were tried to be correlated, and h_{LFP} has not been tried to be correlated before [8]. In the present study, q_{LFP} and h_{LFP} (instead of ΔT_{LFP}) are correlated. This is the new correlation approach. In the recent studies, correlation formats for Equations (2)–(4) were approved to correlate q_{LFP}, h_{LFP}, and ΔT_{LFP}, respectively. The primary items in these equations could be plotted versus pressure as shown in Figure 16.

For ΔT_{LFP}, as discussed above, there are two difficulties on reliable correlation, which determines it would not be considered to be correlated in the current stage. The first one is, as shown in Figures 13 and 16, parameter combination, with the increase of pressure from ambient to around 2.5 MPa, E_{LFP} in Equation (4) shows the increasing-decreasing manner, which indicates that it could not represent the effects of pressure. On the other hand, with the increase of pressure, the variations of ΔT_{LFP} show different manners for various L_{se}. The primary reason is E_{LFP} and Equation (4) are approved for pool boiling in ambient-pressure, which could not be applied in high pressure cases.

For both dominant point and dominated points, q_{LFP} and h_{LFP} are well correlated on the vertical section. This is primarily because the basic effects including pressure, L_{se}, and circumferential position are well involved. At first, for dealing with the effect of circumferential position, dominant points were identified from dominated points, and they were correlated apart from each other. On the other hand, the effects of pressure and L_{se} are involved well in Equations

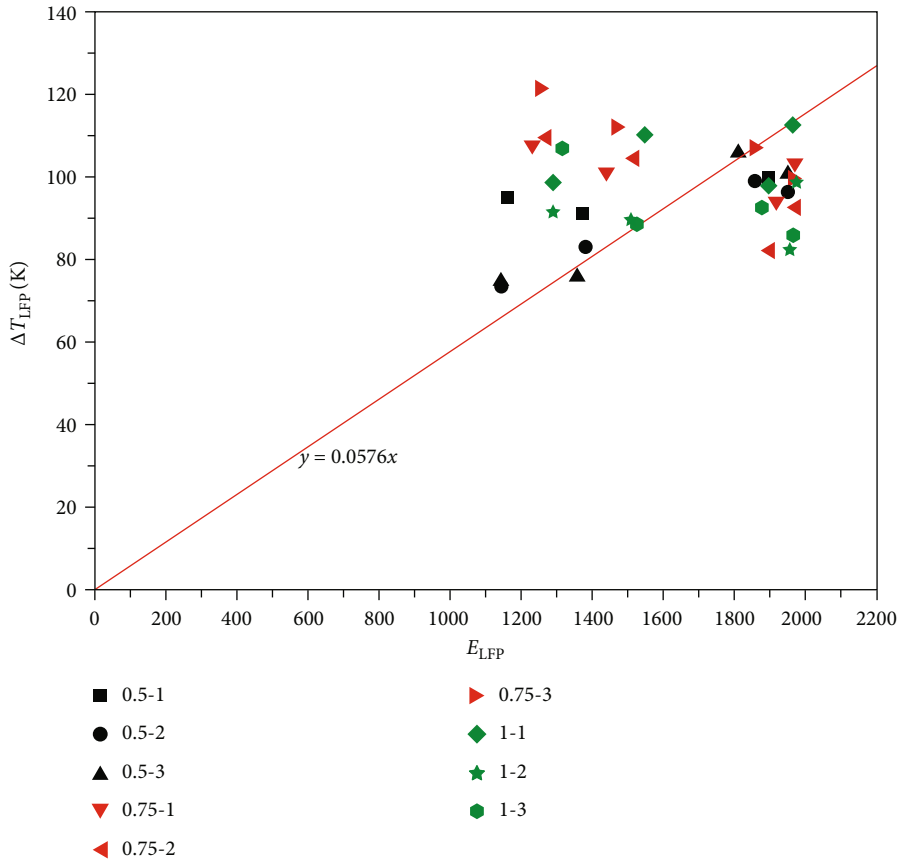

Figure 13: Experimental ΔT_{LFP} versus E_{LFP}.

(2)–(3) and Equations (8)–(9). Especially, as shown in Figure 16, in the effective LFP pressure range from ambient to around 2.5 MPa [8], the primary items in both Equations (2) and (3) (as well as (8) and (9)) increase consistently with the increase of pressure, which indicates that these equations could represent the effect of pressure well.

5. New Correlation on q_{CHF} and Discussions on the Critical Heat Flux Point

5.1. Basic Effect of A_{inj}. Figure 17–19 shows the basic experimental data, where ΔT_{CHF}, q_{CHF}, and h_{CHF} are plotted versus A_{inj}, respectively. With the decrease of A_{inj}, ΔT_{CHF} shows the overall decreasing manner, and both q_{CHF} and h_{CHF} show the overall increasing-decreasing manner, primarily. This is similar with the results in the previous study for horizontal exit-contracted pipe [29].

5.2. Evaluations on the Previous Correlations. In the previous studies, Equation (10) from transport pipe was recommended by the present authors to predict ΔT_{CHF} for horizontal exit-contracted pipe [8, 28]. However, this equation was demonstrated to produce great deviations when predicting the previous set of data, where more detailed T_o was measured [29].

$$\Delta T_{CHF} = T_{CHF} - T_{sat} = 1.345 \times 10^{-5} B, \tag{10}$$

$$B = H_{vl}\rho_v \left[\frac{g\sigma_{vl}(\rho_l - \rho_v)}{\rho_v^2}\right]^{0.25}. \tag{11}$$

Figure 20 plots the experimental ΔT_{CHF} versus parameter B in the present study. These figures show very similar with Figure 13. In this way, similar difficulties on correlations with LFP could be found, which could be discussed next.

In the previous study, new correlations on q_{CHF} have been approved for horizontal exit-contraction pipe [29] as shown in Equation (12) (Equation (13) is another version). This equation involves the effects of L_{se} and circumferential by constant C_3, the effects of u_l by $u_l^{-0.1149}$, and the effects of fluid properties by other items. In the present study, q_{CHF} values could be correlated by Equation (13) as shown in Figure 21, where the constant C_3 could be listed in Table 4, which indicates correlation equation approved from the horizontal exit-contracted pipe would be used in the present vertical exit-contracted pipe.

$$q_{CHF} = C_3 u_l^{0.1149} \rho_v^{0.1262} H_{vl}((\rho_l\text{-}\rho_v)\sigma_{vl})^{0.1667} \rho_l^{0.5405}, \tag{12}$$

$$\frac{q_{CHF}}{\rho_v H_{vl} u_l} = C_3 \left(\frac{\rho_l}{\rho_v u_l^{0.25}}\right)^{0.8738} \left(\frac{\sigma_{vl}}{\rho_l u_l^2 D_{bu}}\right)^{0.3333}. \tag{13}$$

5.3. New Correlation on h_{CHF}. For LFP, both q_{LFP} and h_{LFP} could be correlated by the existing correlation format. In this

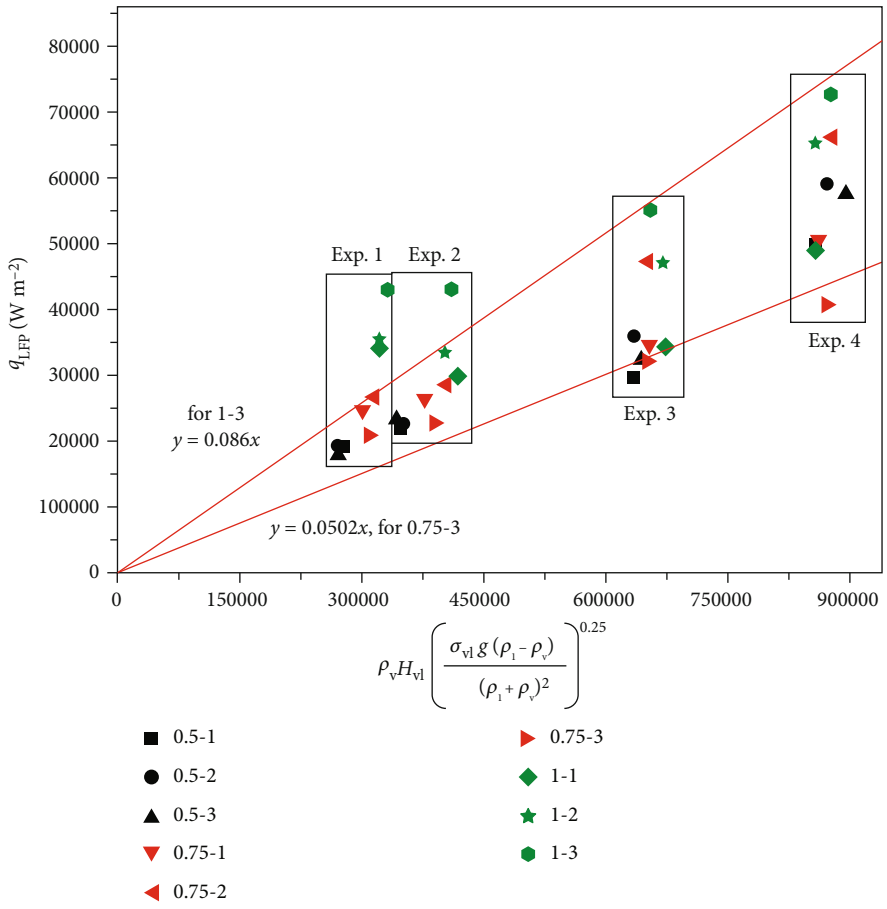

Figure 14: Correlation on q_{LFP} by Equation (2).

Table 4: Constants for every point in Equations (2), (3) and (11), respectively.

Point	Constant C_1	MAE (%)	Constant C_2	MAE (%)	C_3	MAE (%)
0.5-1	0.0555	14.28	0.4828	10.16	0.00703	11.24
0.5-2	0.0643	7.12	0.573	6.29	0.00982	4.06
0.5-3	0.0607	11.20	0.5236	6.26	0.00828	4.06
0.75-1	0.0597	14.05	0.5281	6.40	0.00769	4.00
0.75-2	0.0748	5.45	0.7139	13.60	0.00835	4.19
0.75-3	0.0502	12.26	0.4121	5.72	0.00428	13.65
1-1	0.0572*	10.49	0.4967*	7.09	0.00683	1.53
1-2	0.0749*	6.05	0.7384*	8.74	0.00725	1.63
1-3	0.086*	8.02	0.8264	4.47	0.00994	5.57

*, except Exp. 1.

way, ΔT_{LFP} could be obtained correspondingly. This approach could be adopted when discussing CHF point. In this way, the possibility of correlating h_{CHF} should be evaluated well. Basically, a number of correlations on heat transfer coefficient for nucleate boiling were approved in the previous studies.

Forster-Zuber correlation was applied widely to predict heat transfer for nucleate boiling in pool [36]. In this correlation, the variation between saturation pressure on T_i (temperature inner wall), P_{si}, and P_p (pressure in the pipe) was assumed to vary linearly versus subcooling ΔT_i, $(T_i - T_{sat})$, as Equation (14) shows. In this way, heat transfer coefficient could be predicted by Equation (15), where constant C_4 indicates $C \cdot k_{FZ}{}^{0.75}$. Experimental results show that in the present study, most T_{CHF} values are higher than the critical temperature, which gives the constant P_{si} values. Of course, another possibility is this series of equations were approved for low-pressure cases. Nevertheless, this reduces the role of k_{FZ} as shown in Equation (14), and the effects of k_{FZ} could be just represented by C_4 in Equation (15).

$$P_{si} - P_p = k_{FZ} \Delta T_i, \tag{14}$$

$$h_{NB} = C_4 \frac{\rho_l^{0.5} c_{pl}^{0.125} k_l^{1.125} \mathrm{Pr}_l^{0.333}}{\rho_v^{0.25} H_{vl}^{0.25} \mu_{vl}^{0.625} \sigma_{vl}^{0.5}} \Delta T_i. \tag{15}$$

Comparison shows that, as shown in Equation (15), for CHF, with the increase of pressure, $\rho_l^{0.5} c_{pl}^{0.125} k_l^{1.125} \mathrm{Pr}_l^{0.333} / \rho_v^{0.25} H_{vl}^{0.25} \mu_{vl}^{0.625} \sigma_{vl}^{0.5}$ shows the overall increasing manner;

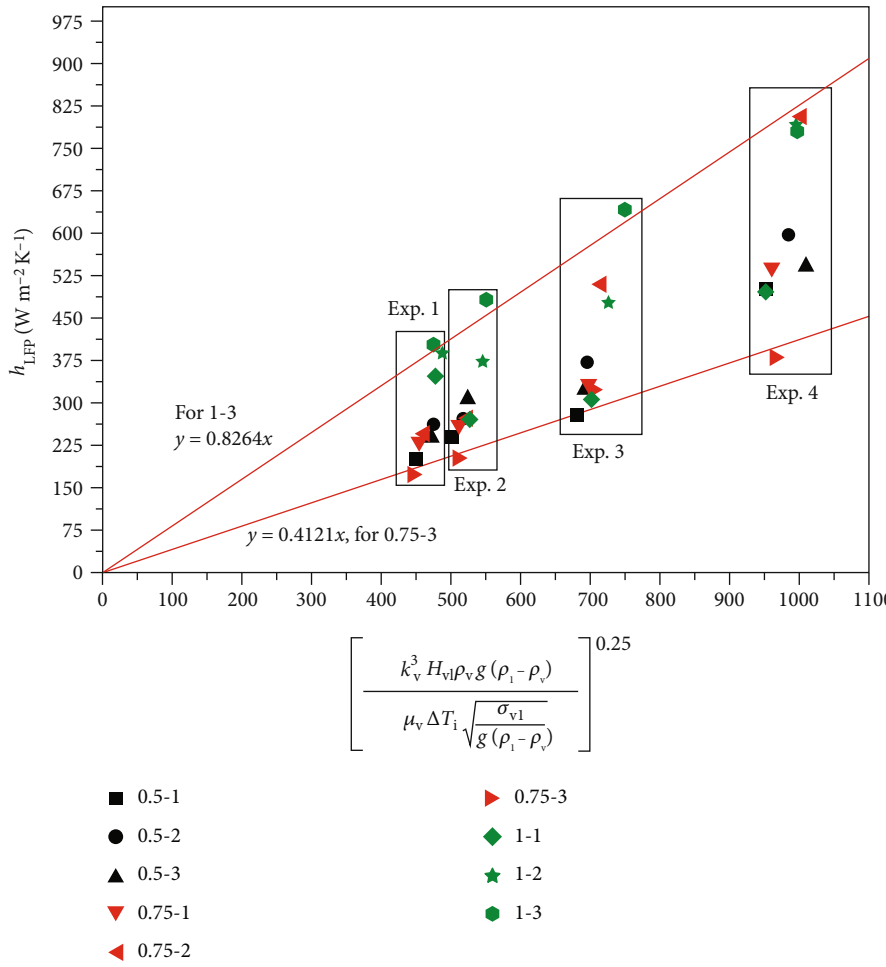

Figure 15: Correlation on h_{LFP} by Equation (3).

however, ΔT_{CHF} shows the contrary manner, which produces extra difficulties on correlation. In this way, the parameter combination could be revised as Equation (16) shows, and the present set of data could be plotted as shown in Figure 22. It shows that h_{CHF} could be correlated by Equation (17), which produces the overall MAE of 2.3% and the max deviation 13.4%. The deviation bar has been plotted in the figure, where the red lines show the ±2% deviation on the present figure, and ±17.9% for the h_{CHF} data.

$$h_{CHF} = C_4 \left(\frac{\rho_v^{0.25} H_{vl}^{0.25} \mu_{vl}^{0.625} \sigma_{vl}^{0.5}}{\rho_l^{0.5} c_{pl}^{0.125} k_l^{1.125} \mathrm{Pr}_l^{0.333}} \Delta T_{CHF} \right)^N, \quad (16)$$

$$h_{CHF} = 19511.9 \left(\frac{\rho_v^{0.25} H_{vl}^{0.25} \mu_{vl}^{0.625} \sigma_{vl}^{0.5}}{\rho_l^{0.5} c_{pl}^{0.125} k_l^{1.125} \mathrm{Pr}_l^{0.333}} \Delta T_{CHF} \right)^{0.6588}. \quad (17)$$

5.4. Primary Effect Factors. Similar with LFP, the effects of pressure, L_{se}, and circumferential positions would be discussed in the present section.

5.4.1. The Effect of A_{inj} or Pressure. CHF point could be recorded in a wide range from the ambient-pressure to around 4.0 MPa. Basically, as shown in Section 5.1, in this pressure range, with the decrease of A_{inj} (increase of pressure), primarily, q_{CHF}, ΔT_{CHF}, and h_{CHF} show the overall constant or increase-decrease manner. These factors are consistent to those approved in the previous studies [8, 29].

5.4.2. The Effects of L_{se}. For LFP, at least q_{LFP} shows the obviously decreasing manner with the increase of L_{qf}. However, for the experimental data on q_{CHF} and h_{CHF}, the effects of L_{se} do not show the obvious regulations. In this way, correlations on these parameters do not involve L_{se}. At least, this indicates L_{se} plays ignorable roles on bubble separation.

5.4.3. The Effects of Circumferential Position. The effect of circumferential position on CHF is similar to that of LFP. As shown in Table 3, for every L_{se}, t_{CHF} values for various circumferential positions (1, West; 2, South; 3, East) are quite similar to others. This indicates that the propagation of bubble separation "front" circumferentially plays significant roles on the CHF for a certain L_{se} cross-section. In

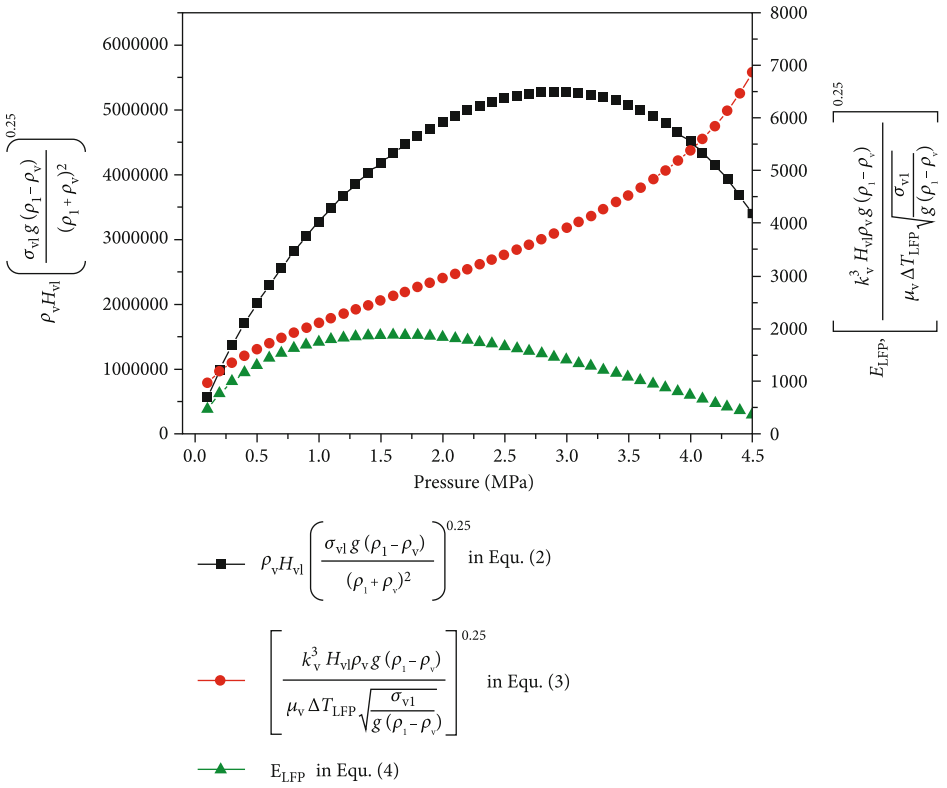

Figure 16: Parameter combinations in Equations (2)–(4) versus pressure.

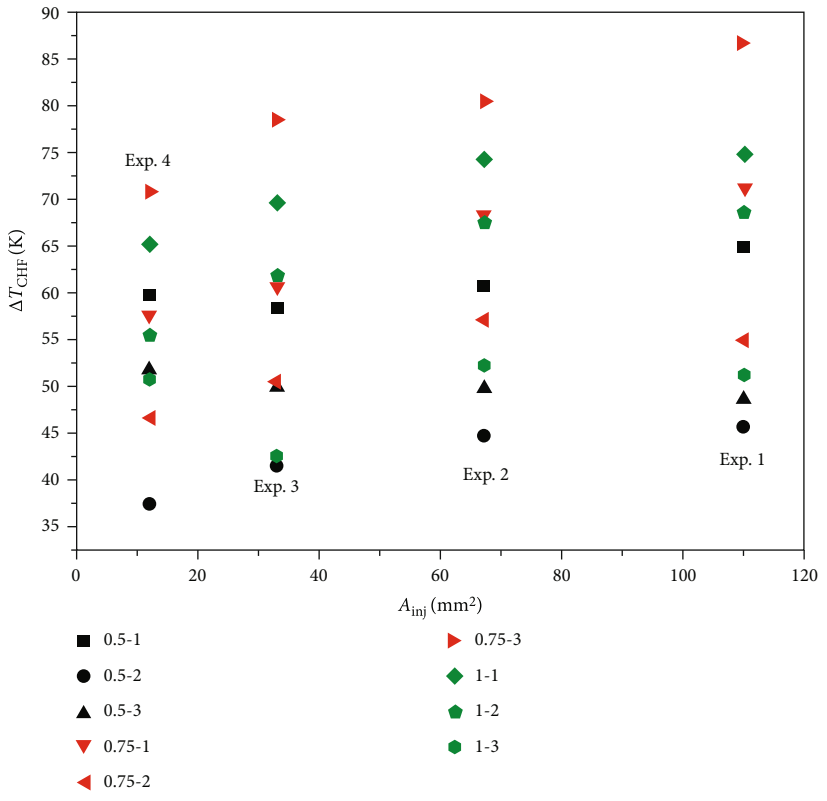

Figure 17: Experimental ΔT_{CHF} versus A_{inj}.

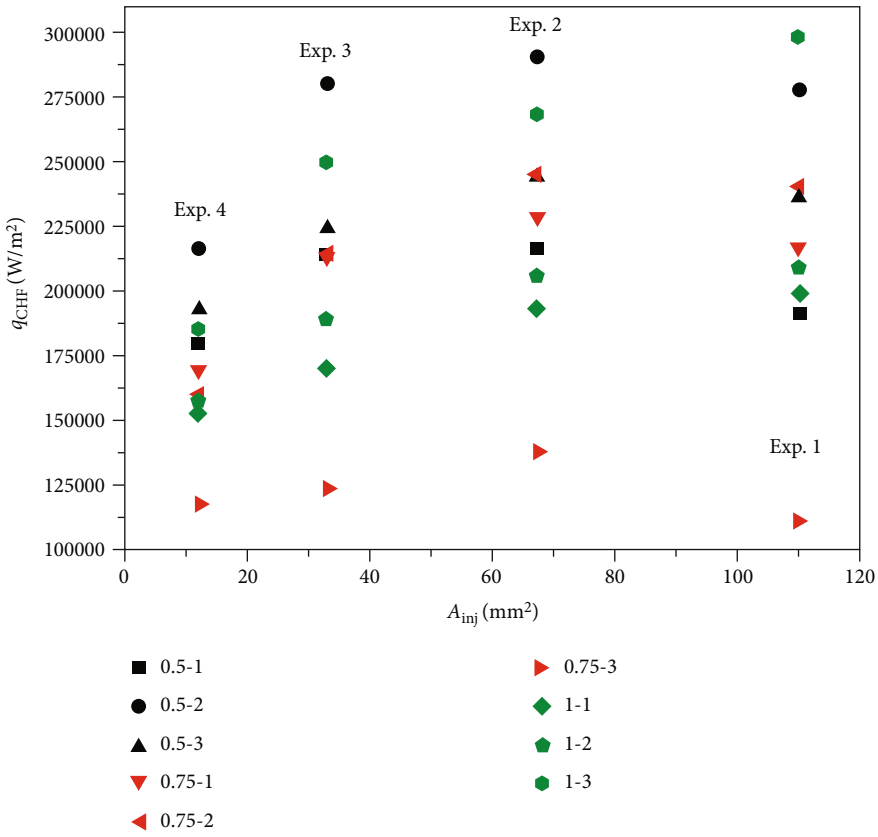

Figure 18: Experimental q_{CHF} versus A_{inj}.

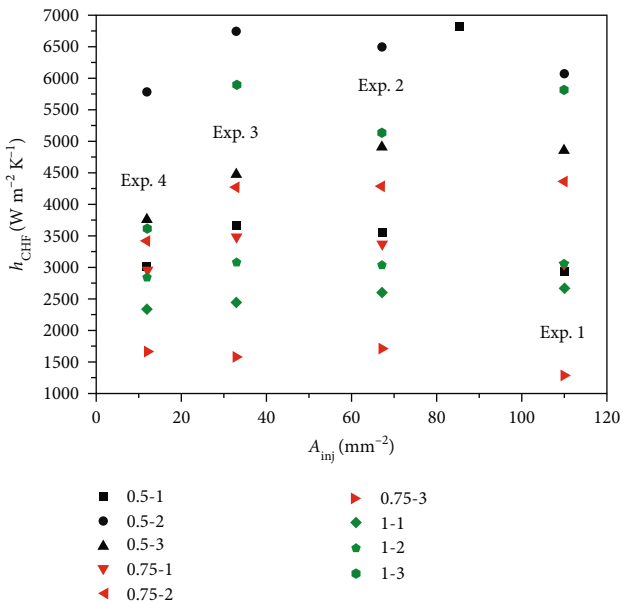

Figure 19: Experimental h_{CHF} versus A_{inj}.

addition, for a certain L_{se}, various circumferential positions are with various q_{CHF}, h_{CHF}, and T_{CHF}. This indicates that, similar with LFP, for a certain L_{se}, there are both dominant point and dominated points. As shown in Table 3, dominant points for bubble separation (CHF), 0.5-2, 0.75-2, and 1-3 are same with those for liquid rewetting (LFP). This is because on the current cross-section, T_i on the dominant point decreases prior to other points, not only on film boiling section but also on transition boiling section. In this way, T_i on the dominant point is always the lowest on the current cross-section and dominates the boiling transitions on the current cross-section.

5.4.4. Summaries on the Basic Factors. As discussed above, the effects of pressure, L_{se}, and circumferential position could be summarized and concluded as follows.

(1) For a certain point, the increase of pressure produces overall decreasing q_{CHF}, h_{CHF}, and deceasing t_{CHF}

(2) The effect of L_{se} plays ignorable roles on CHF, including q_{CHF} and h_{CHF}

(3) Similar with LFP, because of the propagation of bubble separation front circumferentially, on a certain L_{se} (cross-section), there are both dominant point and dominated points, which are controlled by flow instability and both heat transfer and the dominant points. In the present study, 0.5-2, 0.75-2, and 1-3 are the dominant points for these sections, respectively

5.5. Discussions

5.5.1. Correlation on the Dominant Points. From the view of point of correlation, the effects of both pressure and

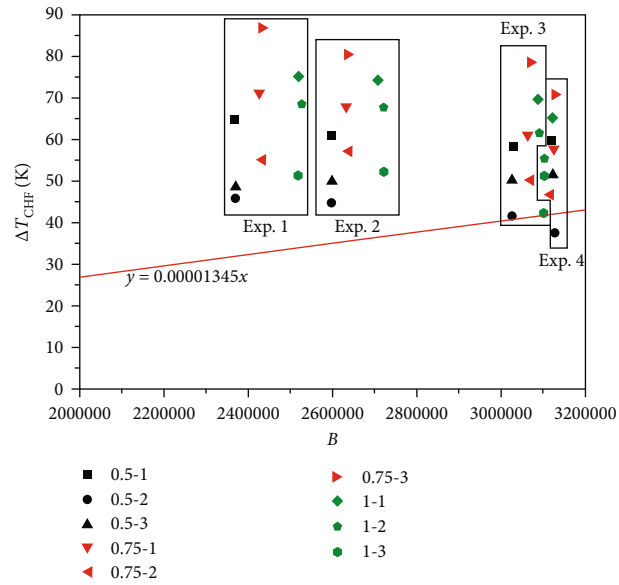

Figure 20: Experimental ΔT_{CHF} versus B.

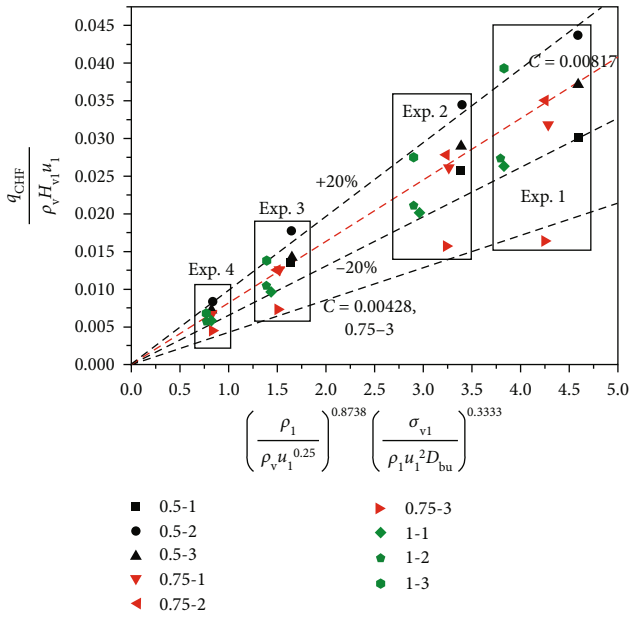

Figure 21: Correlation on q_{CHF} by Equation (12).

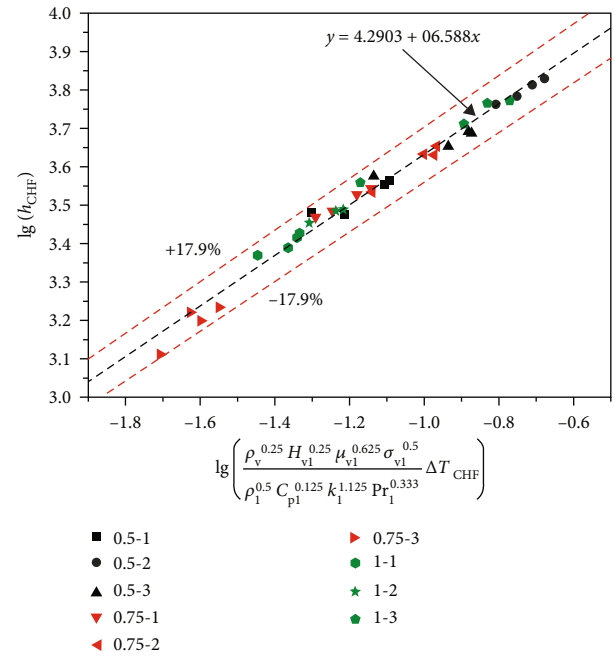

Figure 22: Correlation on h_{CHF} by Equation (17).

circumferential position should be involved. The related strategy is similar with that for LFP, by which the dominant points and dominated points would be discussed, respectively.

As shown in Equation (12) and Table 4, in the present correlation on q_{CHF}, C_3 is correlated to be 0.00982, 0.00835, and 0.00994 for dominant points, 0.5-2, 0.75-2, and 1-3, respectively. This shows that C_3 for 0.5-2 is well consistent to that for 1-3, which shows around 16% greater than that for 0.75-2. Of course, there is also another possibility that 0.75-2 is not the exactly dominant point. Nevertheless, for the dominant points in the vertical section, q_{CHF} could be correlated by Equation (12), in which C_3 could be suggested to be 0.00935, which produces the deviation within ±12%, referring Figure 21.

Correlation format as Equation (12) shows for q_{CHF} is much different from that in the pool boiling, in which q_{CHF} was correlated to be linear versus parameter B as shown in Equation (11) [37]. Equation (12) was approved by the present authors, which represents the effects of bubble size and fluid properties by parameter combination and the effects of L_{se} and circumferential position by C_3 [29]. Figure 21 shows that on the dominant points of the vertical section, q_{CHF} is primarily controlled by bubble size and fluid properties, which are determined primarily by system pressure. In this way, on the vertical section of the present study, q_{CHF} could be well correlated by Equation (12) with the C_3 of 0.00935. Here, previous flow instability theories could not be used here, which has been discussed before [29].

On the other hand, Equation (17) gives good correlations on h_{CHF} for both dominant points and dominated points. With the increase of pressure, all of the parameters including q_{CHF}, ΔT_{CHF}, and h_{CHF} show the overall decreasing manner. In this way, a new parameter combination has been set up referring F-Z equation, as shown in Equation (16), and reliable correlations have been obtained by Equation (17).

5.5.2. Correlation on the Dominated Points. In the current stage, Equation (12) and C_3 listed in Table 4 could be suggested to predict q_{CHF} values for the dominated points. Similar with LFP, on this sort of points, bubble separation is not caused by local flow instability. Result indicates that at t_{CHF}, bubble separation happens on the dominant point of the current cross-section. Almost simultaneously, bubbles are

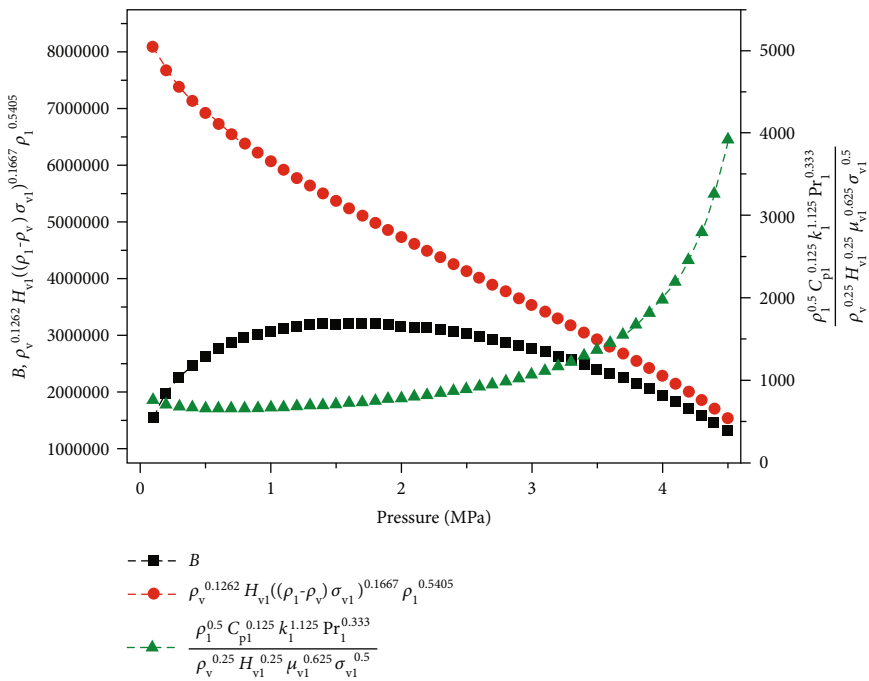

Figure 23: Pressure versus parameter combinations for CHF.

separated from the inner wall on all of this cross-section as a result of bubble separation front propagation circumferentially. In this way, on the dominated points, as a result of being separated, q_i, h_i, and T_i at t_{CHF} have to be denoted as parameters on CHF.

5.5.3. Correlation Formats and Analyses. In the previous studies, q_{CHF} and ΔT_{CHF} were always correlated [8]. However, in the present study, q_{CHF} and h_{CHF} were tried to be correlated instead of ΔT_{CHF}. This is the new correlation approach, similar with LFP. The primary parameter combinations in Equation (11), (12), and (17), used to predict ΔT_{CHF}, q_{CHF}, and h_{CHF}, respectively, could be plotted versus pressure in Figure 23.

As shown in Figure 23, for ΔT_{CHF}, the correlation difficulties are more or less similar to those for ΔT_{LFP}. The key point is the primary parameter combination B in Equation (11) could not represent the effect of pressure.

For q_{CHF}, analysis shows that the effects of pressure and circumferential position should be involved. In the present study, the strategies are similar with those for LFP. For involving the effect of circumferential position, dominant points and dominated points are identified. Results show that q_{CHF} could be well correlated by Equation (12). For three dominant points, C_3 in Equation (12) is approved to be 0.00935, and for dominated points, C_3 in Equation (12) is listed in Table 4. On the other hand, parameter combination in Equation (12) decreases linearly with the increase of pressure as shown in Figure 23. This indicates the effect of pressure, determining bubble size, and fluid properties could be represented well by this correlation.

For h_{CHF}, Equation (17) could be suggested for both dominant points and dominated points. It shows that on the vertical section, it is determined by ΔT_{CHF} and fluid properties, which are dominated by pressure.

6. Conclusion

LO_2 chill-down in a vertical exit-contracted pipe was studied experimentally. Wall temperature was detected in detail (various L_{se} and circumferential position, 1-east, 2-south, and 3-west) to investigate the filling and chill-down process. The filling and chill-down process was described in detail, on which the propagation of quenching front (QF) was detected. Two QFs were found, one for the exit QF and another for the inlet QF. It has been found that the chill-down process is controlled mainly by the formation and propagation of QFs, which are determined by the pressure level. Based on the experimental data, q_{LFP}, h_{LFP}, q_{CHF}, and h_{CHF} were correlated, respectively, for the vertical section. Primary conclusions could be listed as follows.

(1) During LO_2 chill-down process in the vertical exit-contracted pipe, both exit QF and inlet QF are detected. Results show that on most cases, the propagation of the exit QF dominates the liquid rewetting for $L_{se} = 0.5$ m and its downstreams

(2) For both LFP and CHF, circumferential position plays significant roles. On the vertical section, because of the proportions of QF or bubble separation front circumferentially, when LFP or CHF happens on the dominant point, LFP or CHF would happen on the same cross-section (dominated points) in a short period. On the dominant points, LFP is controlled by the flow instability, and CHF is controlled by the bubble size and fluid properties.

However, on the dominated points, both LFP and CHF are determined by the dominant points and heat transfer themselves

(3) Both ΔT_{LFP} and ΔT_{CHF} have not been tried to be correlated. A series of difficulties have been discussed. At first, these two parameters are not independent themselves, and they are both determined by other parameters. On the other hand, the current parameter combinations could not represent the effects of pressure in such a wide range of pressure

(4) Equations (8) and (9), involving the effects of pressure and L_{se} could be suggested to predict q_{LFP}, and h_{LFP} on the dominant points. Equations (2) and (3), with the similar formats with Equations (8) and (9) could be suggested to predict q_{LFP} and h_{LFP} on the dominated points by constant in Table 4

(5) For q_{CHF}, Equation (12) would be suggested, with C_3 of 0.00935 for dominant points and C_3 listed in Table 4 for dominated points. Equation (17) could be strongly suggested to predict h_{CHF} for both sorts of points.

Nomenclature

A: Area, m^2
B: Parameter combination in correlations
C: Constant in correlations
c: Specific heat, $J \cdot kg^{-1} \bullet K^{-1}$
D: Diameter, m
E: Parameter combination in correlations
G: Mass flux in the experimental section, $kg \cdot m^{-2} \bullet s^{-1}$
g: Gravity acceleration, $m \cdot s^{-2}$
H: Latent heat or enthalpy, $J \cdot kg^{-1}$
h: Heat transfer coefficient, $W \cdot m^{-2} \cdot K^{-1}$
k: Heat conductivity, $W \cdot m^{-1} \cdot K^{-1}$, or constant in k_{FZ}
L: Distance, m
$\dot{m}$: Mass flow rate, $kg \cdot s^{-1}$
N: Number of data
P: Pressure, Pa
Pr: Prandtl number, $c_p \cdot \mu \cdot k^{-1}$
q: Heat flux, $W \cdot m^{-2}$
Re: Reynolds number, $D_i G \cdot \mu_l^{-1}$
T: Temperature, K
t: Time, s
u: Velocity, m/s
V: Variables mainly represent T_{LFP}, q_{LFP}, T_{CHF}, and q_{CHF} data.

Subscripts

bu: The bubble
CHF: Critical heat flux point
cr: Critical properties
exp: Experimental data
FZ: Forster-Zuber parameter
FB: Film boiling
i: The inner wall of the pipe
inj: Injector on the pipe exit
LFP: Inner wall data of the Leidenfrost point
l: Liquid phase
NB: Nuclear boiling
o: The outer wall of the pipe
p: Fluid in the experimental section, or constant pressure in c_p
peak: Value of the pressure peak
pre: Predicted data by correlations
s: The solid material
sat: Saturation condition
se: From main valve to outer wall temperature sensors
si: Saturation parameter on inner wall temperature
ss: Steady-state condition, the chill-down finishes
v: Vapor phase
vl: From vapor phase to liquid phase.

Greek Symbols

μ: Viscosity, Pa•s
ρ: Density, $kg \cdot m^{-3}$
σ: Surface tension, $N \cdot m^{-1}$
δ: Thickness of film, m.

Data Availability

Data have been uploaded by "supplemental files" with manuscript file.

Conflicts of Interest

The authors declare that they have no conflicts of interest.

Supplementary Materials

In the "Supplementary files" section, a file named "Data_B," including the LFP and CHF data in the format of table has been uploaded with the manuscript. Related description has been given in the precious section "Data Availability." *(Supplementary Materials)*

References

[1] D. Conte, D. Budzyń, H. Burgoyne et al., "Innovative Mars Global International Exploration (IMaGInE) mission," in *AIAA Space 2016*, Long Beach, California, 2016.

[2] E. A. Hurlbert, R. Whitley, M. D. Kelm et al., "International space exploration coordination group assessment of technology gaps for LOx/methane propulsion systems for the global exploration roadmap," in *AIAA Space 2016*, Long Beach, California, 2016.

[3] H. C. Hansen, W. L. Johnson, M. L. Meyer, A. H. Werkheiser, and J. R. Stephens, "Cryogenic fluid management technologies enabling for the Artemis program and beyond," in *ASCEND 2020*, Virtual Event and Cincinnati, Ohio, 2020.

[4] T. D. Smith, M. D. Klem, and K. L. Fisher, "Propulsion risk reduction activities for non-toxic cryogenic propulsion," in *AIAA SPACE 2010 Conference & Exposition*, Anaheim, California, 2010.

[5] T. Polsgrove, D. Thomas, S. Sutherlin, W. Stephens, and M. Rucker, "Mars ascent vehicle design for human exploration," in *AIAA SPACE 2015 Conference and Exposition*, Pasadena, California, 2015.

[6] J. Collins, E. Hurlbert, K. Romig, J. Melcher, A. Hobson, and P. Eaton, "Sea-level flight demonstration and altitude characterization of a LO2/LCH4 based ascent propulsion lander," in *45th AIAA/ASME/SAE/ASEE Joint Propulsion Conference & Exhibit*, Denver, Colorado, 2009.

[7] S. R. Darr, J. W. Hartwig, J. Dong et al., "Two-phase pipe quenching correlations for liquid nitrogen and liquid hydrogen," *Journal of Heat Transfer*, vol. 141, no. 4, 2019.

[8] J. Zhang, K. Wang, and L. Chen, "Characteristics of boiling transitions during liquid oxygen chill-down in a horizontal pipe with an injector on the exit," *Applied Thermal Engineering*, vol. 182, article 116068, 2021.

[9] J. N. Chung, "Cryogenic two-phase flow and boiling heat transfer during pipe chilldown (invited)," in *37th AIAA Thermophysics Conference*, Portland, Oregon, AIAA, 2004.

[10] K. Yuan, Y. Ji, and J. N. Chung, "Cryogenic boiling and two-phase flow during pipe chilldown in earth and reduced gravity," *Journal of Low Temperature Physics*, vol. 150, no. 1-2, pp. 101–122, 2008.

[11] K. Yuan, Y. Ji, and J. N. Chung, "Cryogenic chilldown process under low flow rates," *International Journal of Heat and Mass Transfer*, vol. 50, no. 19-20, pp. 4011–4022, 2007.

[12] J. Chen, R. Zeng, X. Zhang, L. Qiu, and J. Xie, "Numerical modeling of flow film boiling in cryogenic chilldown process using the AIAD framework," *International Journal of Heat and Mass Transfer*, vol. 124, pp. 269–278, 2018.

[13] H. Hu, T. K. Wijeratne, and J. N. Chung, "Two-phase flow and heat transfer during chilldown of a simulated flexible metal hose using liquid nitrogen," *Journal of Low Temperature Physics*, vol. 174, no. 5-6, pp. 247–268, 2014.

[14] R. Shaeffer, H. Hu, and J. N. Chung, "An experimental study on liquid nitrogen pipe chilldown and heat transfer with pulse flows," *International Journal of Heat and Mass Transfer*, vol. 67, pp. 955–966, 2013.

[15] S. R. Darr, H. Hu, N. G. Glikin et al., "An experimental study on terrestrial cryogenic transfer line chilldown I. Effect of mass flux, equilibrium quality, and inlet subcooling," *International Journal of Heat and Mass Transfer*, vol. 103, pp. 1225–1242, 2016.

[16] S. R. Darr, H. Hu, N. G. Glikin et al., "An experimental study on terrestrial cryogenic tube chilldown II. Effect of flow direction with respect to gravity and new correlation set," *International Journal of Heat and Mass Transfer*, vol. 103, pp. 1243–1260, 2016.

[17] L. Jin, C. Park, H. Cho, C. Lee, and S. Jeong, "Experimental investigation on chill-down process of cryogenic flow line," *Cryogenics*, vol. 79, pp. 96–105, 2016.

[18] L. Jin, H. Cho, C. Lee, and S. Jeong, "Experimental research and numerical simulation on cryogenic line chill-down process," *Cryogenics*, vol. 89, pp. 42–52, 2018.

[19] L. Jin, H. Cho, and S. Jeong, "Experimental investigation on line chill-down process by liquid argon," *Cryogenics*, vol. 97, pp. 31–39, 2019.

[20] L. Jin, J. Lee, and S. Jeong, "Investigation on heat transfer in line chill-down process with various cryogenic fluids," *International Journal of Heat and Mass Transfer*, vol. 150, article 119204, 2020.

[21] J. Johnson and S. R. Shine, "Transient cryogenic chill down process in horizontal and inclined pipes," *Cryogenics*, vol. 71, pp. 7–17, 2015.

[22] J. Wang, Y. Li, L. Wang, K. Zhu, F. Xie, and C. Li, "Transient modeling of cryogenic two-phase flow boiling during chill-down process," *Applied Thermal Engineering*, vol. 143, pp. 461–471, 2018.

[23] A. C. LeClair, J. W. Hartwig, D. M. Hauser, M. Kassemi, P. G. Díaz-Hyland, and T. R. Going, "Modeling cryogenic chilldown of a transfer line with the generalized fluid system simulation program," in *2018 Joint propulsion conference*, p. 4756, Virtual Event and Cincinnati, Ohio, 2018.

[24] J. C. Melcher and R. L. Morehead, "Combustion stability characteristics of the project morpheus liquid oxygen/liquid methane main enginE," in *50th AIAA/ASME/SAE/ASEE Joint Propulsion Conference*, Cleveland, OH, 2014.

[25] P. Cui, Q. Li, P. Cheng, and L. Chen, "System scheme design for LOX/LCH4 variable thrust liquid rocket engines using motor pump," *Acta Astronautica*, vol. 171, pp. 139–150, 2020.

[26] R. L. Morehead, J. C. Melcher, M. J. Atwell, E. A. Hurlbert, and P. Desai, "Vehicle-level oxygen/methane propulsion system hotfire demonstration at thermal vacuum conditions," in *53rd AIAA/SAE/ASEE Joint Propulsion Conference*, Atlanta, GA, 2017.

[27] N. Cho, S. Kim, Y. Kim, and S. J. J. Jung, "Two-phase flow characteristics of liquid oxygen flow in low pressure liquid rocket engine," *Cryogenics*, vol. 44, no. 6-8, pp. 493–500, 2004.

[28] J. Zhang, K. Wang, and L. Chen, "Experimental study on liquid oxygen chilldown in the horizontal pipe with an injector on the exit," *Applied Thermal Engineering*, vol. 173, article 115212, 2020.

[29] J. Zhang, K. Wang, and L. Chen, "Experimental study on liquid oxygen chill-down in a horizontal exit-contracted pipe," *Cryogenics*, vol. 120, article 103387, 2021.

[30] H. Hong, N. Jacob, A. Chung, and S. H. Amber, "An experimental study on flow patterns and heat transfer characteristics during cryogenic chilldown in a vertical pipe," *Cryogenics*, vol. 52, no. 4-6, pp. 268–277, 2012.

[31] J. Hartwig, S. Darr, and A. Asencio, "Assessment of existing two phase heat transfer coefficient and critical heat flux correlations for cryogenic flow boiling in pipe quenching experiments," *International Journal of Heat and Mass Transfer*, vol. 93, pp. 441–463, 2016.

[32] N. Zuber, M. Tribus, and J. W. West, "The hydrodynamic crisis in pool boiling of saturated and subcooled liquid," *International Development in HEAT Transfer*, pp. 230–236, 1961.

[33] P. J. Berenson, "Film-boiling heat transfer from a horizontal surface," *Journal of Heat Transfer*, vol. 83, no. 3, pp. 351–356, 1961.

[34] Y. Katto and C. Kurata, "Critical heat flux of saturated convective boiling on uniformly heated plates in a parallel flow," *International Journal of Multiphase Flow*, vol. 6, no. 6, pp. 575–582, 1980.

[35] J. J. Carbajo, "A study on the rewetting temperature," *Nuclear Engineering and Design*, vol. 84, no. 1, pp. 21–52, 1985.

[36] H. K. Forster and N. Zuber, "Dynamics of vapor bubbles and boiling heat transfer," *AICHE Journal*, vol. 1, no. 4, pp. 531–535, 1955.

[37] N. Zuber, "Nucleate boiling. The region of isolated bubbles and the similarity with natural convection," *International Journal of Heat and Mass Transfer*, vol. 6, no. 1, pp. 53–78, 1963.